

Maritime Security as a Global Public Good: Trade Frictions, Chokepoint Vulnerability, and a Scenario Engine Using AIS Shipping Density

Carlos

February 16, 2026

Abstract

This paper frames maritime security as a global public good and evaluates how disruptions at maritime bottlenecks exacerbate trade frictions by rerouting and causing congestion. Using high-resolution AIS ship-density rasters from the IMF World Seaborne Trade Monitoring System ([Cerdeiro et al., 2020](#)), we construct a 78-node maritime transport network—56 major ports, 6 chokepoints, and 16 ocean waypoints connected by approximately 155 edges following real-world shipping corridors—and implement a scenario engine that simulates the consequences of bottleneck closures, capacity reductions, and risk spikes across 1,540 port-to-port trade routes. Under full closure scenarios, the Panama Canal (mean rerouting cost of 17,840 km-equivalent), Gibraltar (10,624 km), and the Suez Canal (9,949 km) generate the largest rerouting costs. Bab el-Mandeb (4,700 km) and the Bosphorus (3,275 km) force traffic onto longer maritime alternatives or expensive overland bypasses at 5 \times normal cost. A partial-capacity degradation exercise and a per-chokepoint security risk analysis demonstrate that even modest disruptions produce economically meaningful increases in trade costs, and that the marginal value of security provision increases with risk. We estimate daily rerouting costs of chokepoint closure ranging from \$16 million (Bab el-Mandeb) to \$233 million (Gibraltar), implying aggregate annual costs on the order of tens of billions of dollars. These findings provide a replicable, data-grounded framework for quantifying the “hegemonic dividend” — the economic value of the provision of systemic global security in the maritime commons of the status-quo.

1 Introduction

1.1 Motivation

Global commerce is overwhelmingly maritime. Approximately 80 percent of world trade by volume and over 70 percent by value traverses the oceans, channeled through a small

number of physical bottlenecks—straits, canals, and narrow sea lanes—that concentrate traffic and vulnerability (Verschuur et al., 2023; Bueger et al., 2024). The reliability of these corridors is not a natural given; it depends on the provision of security, navigational infrastructure, and rules-based governance that together constitute what international relations scholars term the “global maritime commons” (Bueger et al., 2019; Kraska, 2015). When this security breaks down—through piracy, conflict-related closures, or geopolitical risk—the consequences propagate rapidly through rerouting, congestion, and elevated trade costs (Besley et al., 2015; Notteboom, 2006).

The U.S. Navy has historically been the predominant provider of security in the global commons, maintaining forward presence through overseas basing, freedom of navigation operations (FONOPs), and patrol activities that deter threats and ensure the openness of critical sea lanes. This role can be framed as the provision of a *global public good*: security that is non-rival (one country’s benefit from safe sea lanes does not diminish another’s) and largely non-excludable (all trading nations benefit from open chokepoints regardless of contribution) (Bueger et al., 2024; Mbekeani and Ncube, 2011). The economic value of this public good—what we term the “hegemonic dividend”—remains poorly quantified, in part because the most policy-relevant outcomes (trade reliability, routing resilience, avoided cost spikes) are *equilibrium objects* of a transportation network that require explicit modeling of route substitution.

1.2 Research Question and Approach

This paper asks: *How sensitive is the global maritime trading system to disruptions at critical chokepoints, and what is the economic value of security provision that prevents or mitigates such disruptions?*

Figure 1 provides the motivating empirical context: global AIS ship-density data reveal that maritime traffic is extraordinarily concentrated along a small number of corridors, funneling through physical bottlenecks where disruption risk is highest.

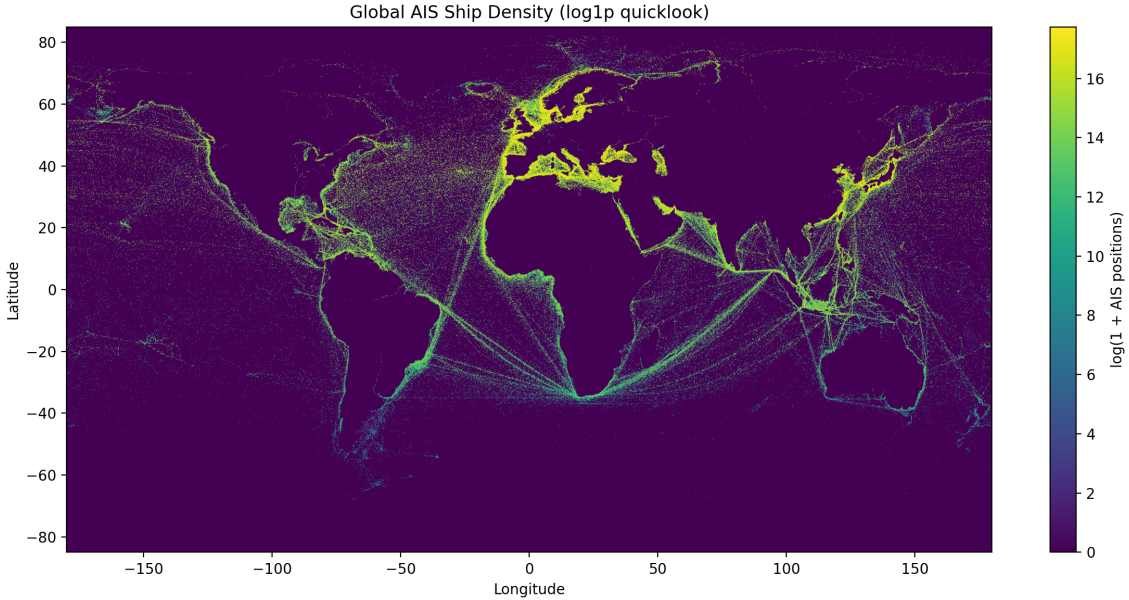


Figure 1: Global AIS ship-density raster (log scale), aggregating vessel position reports from January 2015 to February 2021. Traffic concentrates along established corridors and funnels through a small number of physical chokepoints. Data from the IMF World Seaborne Trade Monitoring System ([Cerdeiro et al., 2020](#)).

We address this question through a scenario-based quantitative spatial framework rather than through direct causal estimation of naval operations. This choice is motivated by two considerations. First, granular data on naval deployments, patrol schedules, and operational details are largely classified and unavailable for academic research. Second, even with such data, the most informative exercise for policymakers is counterfactual: *what would happen if a chokepoint were disrupted, and how much would enhanced security reduce the losses?* This framing aligns with the “transportation networks” approach in quantitative spatial economics ([Fajgelbaum and Schaal, 2020a](#); [Allen and Arkolakis, 2022](#)), which represents trade flows on a graph with endogenous route choice and congestion, and evaluates counterfactuals by shocking network elements and recomputing equilibrium.

Our empirical strategy proceeds in three stages. First, we use high-resolution AIS (Automatic Identification System) ship-density rasters from the IMF World Seaborne Trade Monitoring System ([Cerdeiro et al., 2020](#)) to construct a baseline portrait of global shipping intensity and to measure the concentration of maritime activity at six major chokepoints. Second, we build a stylized maritime transport network—a weighted graph of ocean basins and chokepoints—in which edge costs depend on distance and a congestion proxy calibrated from the AIS density data. Third, we implement a “scenario engine” that imposes exogenous shocks to chokepoint edges (closure, capacity reduction, risk spike) and computes the result-

ing changes in least-cost path lengths, rerouting patterns, and aggregate trade-cost indices across basin pairs. Security enters the model as a cost-reducing and risk-reducing shifter on bottleneck-adjacent edges: higher security provision lowers the effective cost of transit and improves reliability, which becomes especially valuable under disruption scenarios.

1.3 Contributions

This paper makes three contributions. First, it provides a replicable, data-grounded measurement framework for evaluating chokepoint vulnerability using publicly available AIS data. The global density map and chokepoint intensity rankings we construct offer a transparent baseline for any subsequent analysis of maritime disruptions. Second, the scenario engine translates the qualitative intuition that “chokepoints matter” into quantitative cost-change estimates that can be compared across bottlenecks and shock magnitudes. This ranking of vulnerability—which bottleneck closure generates the largest rerouting cost—is directly useful for security resource allocation. Third, by situating the analysis within the quantitative spatial economics toolkit ([Redding and Rossi-Hansberg, 2017](#); [Donaldson, 2025](#)), we connect the maritime security literature to a rigorous modeling tradition that emphasizes general-equilibrium effects, welfare measurement, and network structure.

We are explicit about the limitations of the current exercise. With only an aggregate density raster (not vessel-level trajectories or bilateral trade flows), we cannot estimate a full spatial equilibrium with origin-destination demand or compute welfare in the general-equilibrium sense of [Fajgelbaum and Schaal \(2020a\)](#). The network model is therefore stylized: it uses great-circle distances for edge weights, a congestion proxy derived from raster intensity, and shortest-path routing. We label all scenario results as “partial-exercise” estimates and interpret them as informative bounds on the sensitivity of the maritime system to disruption. A key output of the paper is a concrete specification of what additional data—vessel-level AIS trajectories, bilateral maritime trade matrices, insurance risk indicators, and naval presence measures—would be needed to move from scenario simulation to causal inference.

1.4 Roadmap

Section 2 reviews the literature on maritime security as a public good, trade frictions and risk, quantitative spatial models of transportation, and the use of AIS data in economic research. Section 3 describes the data (AIS density raster, chokepoint definitions) and methods (network construction, cost specification, scenario design). Section 4 presents results: baseline density patterns, chokepoint intensity rankings, and scenario outputs under multiple

shock types. Section 5 discusses implications, limitations, and directions for future work.

2 Literature Review

This literature review synthesizes scholarly work across five domains that jointly motivate and inform the present analysis: maritime security as a global public good; the economics of trade frictions, risk, and piracy; quantitative spatial models of trade and geography; transportation network models with congestion; and emerging data sources in maritime economics. We also draw on the broader spatial economics literature on optimal policy, agglomeration, and redistribution to frame the welfare implications of security provision.

2.1 Maritime Security as a Global Public Good

The concept of maritime security as a global public good is central to international relations and security studies. [Bueger et al. \(2019\)](#) argue for a holistic understanding of maritime security that links national, environmental, economic, and human dimensions, establishing that the “politics of the global sea” are fundamentally under-theorized relative to their economic importance. In a comprehensive assessment, [Bueger et al. \(2024\)](#) emphasize that global trade, energy security, and food security all depend on safe and secure oceans, and that the provision of this security exhibits classic public-good characteristics: non-rivalry and partial non-excludability.

The legal foundations of maritime security are grounded in the international law of the sea. [Kraska \(2015\)](#) provides a detailed treatment of the legal framework governing freedom of navigation, passage through straits, and the rights and obligations of naval forces in international waters. This framework underpins the legitimacy of forward naval presence as a security provider and defines the legal space within which chokepoint governance operates.

From a defense economics perspective, military spending on maritime security can be understood as an investment in institutional infrastructure for the global economy. The economic cost of maritime insecurity has been documented in several contexts. [Mbekeani and Ncube \(2011\)](#) estimate the direct economic impacts of piracy for African development, including higher insurance costs, rerouting expenses, and deterrence of investment. The One Earth Future Foundation’s report on the economic cost of piracy ([One Earth Future Foundation, 2010](#)) provides a comprehensive accounting of piracy-related costs including ransoms, insurance, naval patrols, and supply-chain disruptions, estimating annual global costs in the billions of dollars.

2.2 Trade Frictions, Risk, and Maritime Disruptions

The project’s focus on trade frictions arising from security risk connects to a broad literature on the determinants and consequences of trade costs. [Besley et al. \(2015\)](#) provide a landmark study of the welfare costs of lawlessness in the context of Somali piracy, showing that piracy acts as a significant cost shifter for international shipping routes. Their identification strategy exploits the spatial and temporal variation in piracy risk to estimate the impact on shipping costs and trade flows, establishing a direct empirical link between maritime insecurity and economic outcomes.

Disruptions at maritime chokepoints represent a particularly consequential form of trade friction because they affect not individual routes but the entire network structure. [Verschuur et al. \(2023\)](#) analyze the systemic economic impacts of disruptions at 24 major maritime chokepoints and estimate potentially large global losses, with some scenarios involving GDP impacts of several percentage points for vulnerable economies. Their findings provide strong motivation for a scenario-based modeling approach and establish that chokepoint disruptions propagate through the global economy via complex network effects.

The port congestion literature provides relevant evidence on how capacity constraints translate into economic costs. [Nottiboom \(2006\)](#) analyzes the relationship between port congestion and freight rates, demonstrating that congestion at key nodes produces cost increases that ripple through the shipping industry. [Du et al. \(2020\)](#) offer a broader assessment of port congestion’s economic impacts and policy responses, documenting the strategies that ports employ to manage delays and their effectiveness.

2.3 Quantitative Spatial Economics

The methodological backbone of this paper is the quantitative spatial economics framework, which combines theoretical structure with empirical tractability to evaluate the general-equilibrium effects of infrastructure, policy, and shocks. [Redding and Rossi-Hansberg \(2017\)](#) provide the foundational survey of this field, establishing the canonical framework in which locations differ in productivity and amenities, trade costs govern the flow of goods across space, and equilibrium outcomes depend on the entire spatial distribution of economic activity. This framework has become the workhorse for evaluating transportation, trade, and place-based policies.

[Allen and Arkolakis \(2025\)](#) extend this framework to regional analysis, developing tools for studying how productivity and policy changes propagate across space through trade and migration linkages. [Redding \(2025\)](#) focuses on the urban dimension, showing how the same quantitative tools can be applied to understand within-city spatial structure and commuting

patterns. Together, these surveys establish the methodological vocabulary—iceberg trade costs, gravity-based trade flows, hat-algebra counterfactuals—that we adapt to the maritime setting.

The broader spatial economics literature provides essential context for understanding why location, agglomeration, and connectivity matter. [Duranton and Puga \(2004\)](#) develop the micro-foundations of urban agglomeration economies, identifying the sharing, matching, and learning mechanisms that generate productivity gains from spatial concentration. [Desmet and Henderson \(2015\)](#) study the geography of development within countries, showing that spatial variation in productivity and access to markets drives large differences in living standards even within national borders. [Proost and Thisse \(2019\)](#) offer a synthetic assessment of what can be learned from spatial economics, emphasizing the field’s ability to evaluate policies with spatial dimensions—a category that naturally includes maritime security.

2.4 Transportation Networks and Congestion

The core analytical engine of our paper draws on the transportation networks literature within spatial economics. [Fajgelbaum and Schaal \(2020a\)](#) develop the foundational framework for analyzing optimal transport networks in spatial equilibrium, in which a planner allocates infrastructure investment across edges of a network to maximize welfare, subject to the constraint that trade flows and route choices are endogenous to the resulting cost structure. Their model demonstrates that optimal networks concentrate investment on high-traffic corridors—a finding with direct parallels to the concentration of maritime activity at chokepoints. The online supplement ([Fajgelbaum and Schaal, 2020b](#)) provides the computational details that inform our own implementation.

[Allen and Arkolakis \(2022\)](#) develop a quantitative spatial model with endogenous traffic congestion and apply it to the U.S. highway network. Their framework—in which edge costs are increasing in traffic through a congestion function—provides a close methodological parallel to our maritime cost specification, where chokepoint edge costs depend on shipping intensity. The welfare effects they estimate from highway improvements establish the empirical relevance of congestion-based cost functions for infrastructure evaluation.

[Donaldson \(2025\)](#) offers a comprehensive survey of transport infrastructure evaluation methods, providing a template for applied policy analysis that our paper follows. His emphasis on distinguishing between identified causal effects and model-based counterfactuals is directly relevant to our approach, which is transparent about operating primarily in the counterfactual simulation domain.

[Hierons \(2024\)](#) studies optimal congestion pricing in general equilibrium, developing a framework in which a planner sets tolls on congested edges to internalize externalities. This work provides guidance for the “optimal security allocation” extension of our model, in which security resources are allocated across bottlenecks to maximize the reduction in expected trade costs. [Bordeu \(2025\)](#) examines infrastructure investment under political fragmentation, highlighting coordination problems that arise when multiple jurisdictions share a common network—an analogy to the provision of global maritime security when international cooperation is incomplete and a single hegemon bears a disproportionate share of the cost.

2.5 Spatial Policy, Redistribution, and Welfare

The welfare implications of maritime security connect to the broader literature on optimal spatial policies. [Fajgelbaum and Gaubert \(2020\)](#) develop the theory of optimal spatial policies in the presence of geographic sorting, showing how place-based interventions interact with spatial equilibrium to produce welfare gains or losses. [Fajgelbaum and Gaubert \(2025\)](#) extend this analysis in a handbook chapter that surveys the frontier of optimal spatial policy design. [Fajgelbaum et al. \(2019\)](#) study how state-level tax differences create spatial misallocation in the United States, establishing that policy-induced distortions to location choices can have first-order welfare effects—a finding that extends naturally to maritime corridors where security differentials affect route choice.

[Gaubert et al. \(2025\)](#) analyze place-based redistribution, developing tools for evaluating the equity and efficiency implications of spatially targeted policies. [Owens et al. \(2020\)](#) apply spatial economic tools to the case of Detroit, demonstrating how place-based interventions can be evaluated within a quantitative spatial framework. [Rossi-Hansberg \(2004\)](#) studies optimal urban land use and zoning, providing foundational theory for how spatial planners should allocate resources across locations—an intellectual ancestor of the “optimal security allocation” problem we pose. [Rossi-Hansberg et al. \(2023\)](#) examine how the spatial distribution of cognitive activity (“cognitive hubs”) affects the case for spatial redistribution, establishing that agglomeration externalities create a role for policy even in market economies.

[Rossi-Hansberg \(2020\)](#) provides a compact analytical treatment of transportation network models that highlights the key features delivering tractability: sparse network structure, congestion-based costs, and shortest-path or logit routing. These features are directly incorporated into our maritime network specification.

2.6 AIS Data and Measurement in Maritime Economics

The empirical implementation of this paper relies on Automatic Identification System (AIS) data, which have become a cornerstone of modern maritime economics research. Kerbl (2022) provides an overview of the use of AIS data in economic research, documenting the range of applications from trade measurement to congestion analysis and highlighting both the opportunities and the challenges (coverage gaps, vessel identification, large data volumes) that researchers face.

Cariou and Cheaitou (2021) use AIS data to study the economic impact of the COVID-19 shock on container flows and ship waiting times in major ports, illustrating how AIS supports real-time measurement of disruptions and their propagation through the maritime network. Cerdeiro and Komaromi (2020) combine AIS data with machine learning techniques to nowcast world trade, demonstrating the predictive content of shipping movements for macroeconomic outcomes. Together with the IMF World Seaborne Trade Monitoring System (Cerdeiro et al., 2020) that provides our primary dataset, these papers establish the feasibility of constructing key model inputs—traffic flows, congestion proxies, and activity intensity measures—from AIS data.

Morabito (2023) provides a comprehensive treatment of maritime transport economics in a doctoral thesis that covers market structure, pricing, and the economics of port competition—offering institutional detail that contextualizes our network model within the operational realities of the shipping industry.

2.7 Summary and Gap

This literature review reveals a clear foundation for modeling maritime security as a public good with measurable economic value. The quantitative spatial economics toolkit (Redding and Rossi-Hansberg, 2017; Allen and Arkolakis, 2025) provides the theoretical structure; transportation network models (Fajgelbaum and Schaal, 2020a; Allen and Arkolakis, 2022) supply the analytical engine; and AIS data (Kerbl, 2022; Cerdeiro et al., 2020) enable empirical measurement. Yet a gap remains: existing work rarely combines a global maritime network model with endogenous rerouting and congestion to value security provision under counterfactual disruptions. The chokepoint vulnerability literature (Verschuur et al., 2023) establishes the stakes but typically relies on reduced-form or input-output methods rather than network-equilibrium counterfactuals. The piracy literature (Besley et al., 2015; One Earth Future Foundation, 2010) quantifies costs but treats routes as fixed rather than endogenous. Our paper aims to bridge this gap by combining insights from the transportation networks tradition with AIS-based measurement and a flexible scenario framework that

accommodates the full range of bottleneck disruptions relevant to maritime security policy.

3 Data and Methods

3.1 Data

3.1.1 AIS Ship Density Raster

Our primary data source is the global ship density raster from the IMF World Seaborne Trade Monitoring System ([Cerdeiro et al., 2020](#)). The dataset aggregates AIS (Automatic Identification System) position reports received between January 2015 and February 2021 into a global raster grid at $0.005^\circ \times 0.005^\circ$ resolution (approximately 500m \times 500m at the equator). Each cell records the total number of AIS positions reported within that cell over the entire period, covering both moving and stationary vessels. The raster thus measures the *intensity of shipping activity* at each location—a proxy for the cumulative traffic load experienced by each point in the global ocean.

The dataset is distributed as a single GeoTIFF file (approximately 9 GB) with pre-computed overview pyramids (approximately 3 GB). The raster covers the full global extent in WGS84 geographic coordinates. Given its size, all processing uses memory-safe techniques: built-in overviews for global visualization, windowed reads for chokepoint-level extraction, and aggressive downsampling (to 3600×1800 pixels) for summary statistics. The AIS data underlying the raster have been validated for use in economic research; see [Kerbl \(2022\)](#) for a discussion of AIS data quality, coverage, and applications, and [Cerdeiro and Komaromi \(2020\)](#) for the IMF’s methodology for constructing trade-relevant indicators from AIS.

3.1.2 Chokepoint Definitions

We define six maritime chokepoints as coarse bounding boxes in geographic coordinates ([Table 1](#)). Each bounding box encloses the navigable channel and approach lanes of a major maritime bottleneck. We extract the AIS density within each bounding box via windowed raster reads and compute aggregate intensity statistics. The six chokepoints are:

1. **Suez Canal** — connecting the Mediterranean and Red Sea;
2. **Bab el-Mandeb** — southern entrance to the Red Sea;
3. **Strait of Malacca** — connecting the Indian Ocean and South China Sea;
4. **Panama Canal** — connecting the Atlantic and Pacific Oceans;
5. **Bosporus** — connecting the Black Sea and Mediterranean;
6. **Strait of Gibraltar** — entrance to the Mediterranean from the Atlantic.

These chokepoints were selected based on their prominence in the maritime security literature (Verschuur et al., 2023; Bueger et al., 2024) and their role as physical bottlenecks that concentrate traffic and create vulnerability. The Strait of Hormuz, the Cape of Good Hope, and the Danish Straits are included in the network as waypoint nodes (enabling realistic routing) but are not classified as chokepoints for the closure analysis: the Strait of Hormuz functions as a critical but open passage without the canal-like physical constraints of Suez or Panama; the Cape of Good Hope is an open-ocean alternative route; and the Danish Straits do not constitute a narrow mandatory-passage bottleneck for modern shipping. The bounding boxes are deliberately coarse to ensure computational tractability and to capture approach-lane traffic in addition to the narrowest passage.

Table 1: Chokepoint Bounding Box Definitions

Chokepoint	Lon Min	Lon Max	Lat Min	Lat Max
Suez Canal	32.20	32.65	29.80	31.30
Bab el-Mandeb	42.25	43.55	12.15	13.25
Strait of Malacca	99.00	104.80	1.00	6.50
Panama Canal	-80.20	-79.40	8.70	9.60
Bosporus	28.90	29.30	41.05	41.25
Gibraltar	-6.20	-5.20	35.80	36.30

Figure 2 illustrates the bounding box extraction procedure using the Suez Canal as an example. The bounding box captures the canal and its approach lanes on the Mediterranean and Red Sea sides, where vessel traffic concentrates into a high-density corridor. The full set of six bounding boxes is shown on a world map in Appendix A (Figure 18).

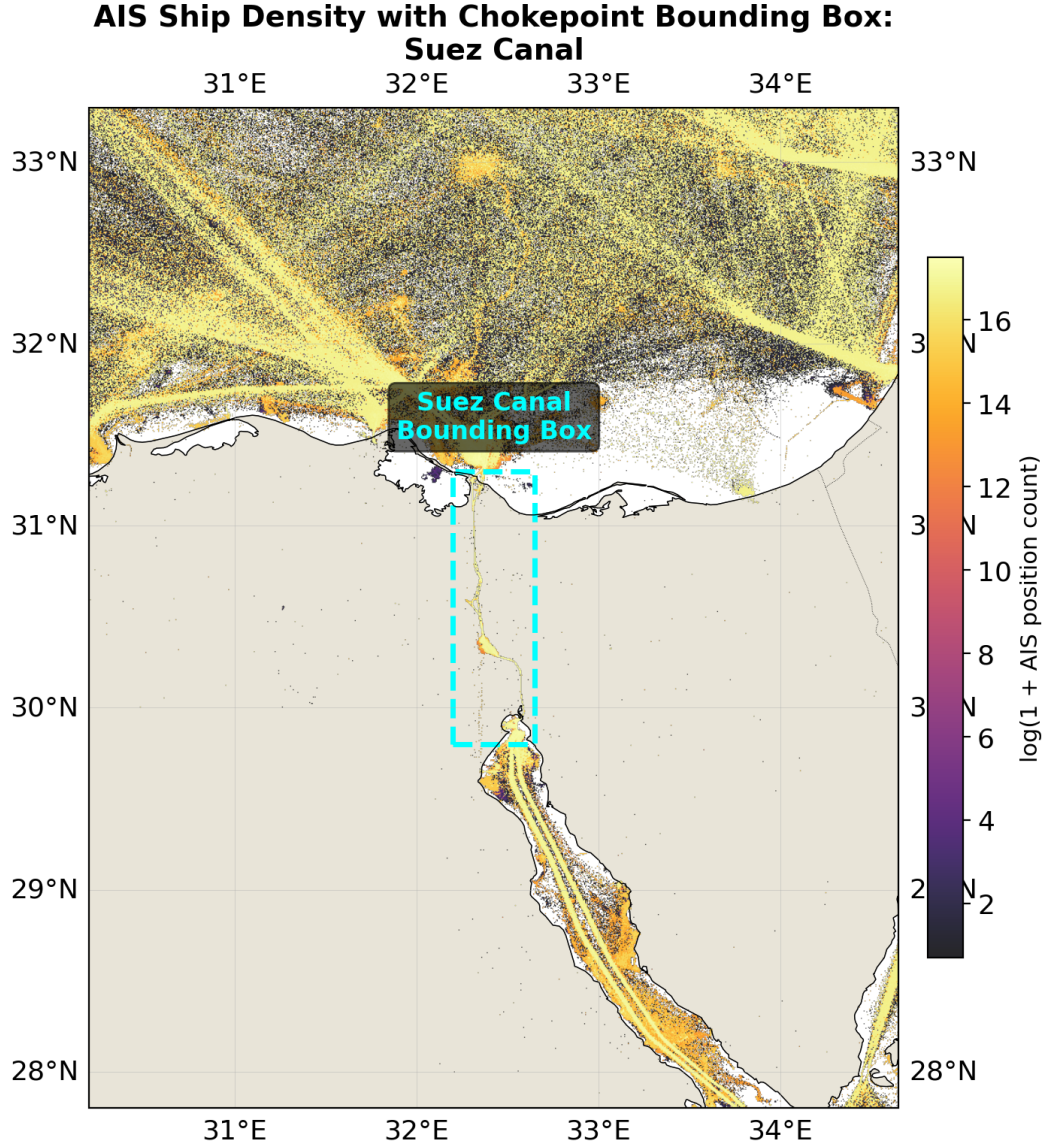


Figure 2: AIS ship density at the Suez Canal with the chokepoint bounding box overlaid (dashed cyan). The heatmap shows log-transformed AIS position counts; brighter areas indicate higher traffic intensity.

3.2 Methods

3.2.1 Empirical Strategy: Bottleneck Scenario Analysis on a Maritime Transport Network

The central challenge in quantifying maritime security as a global public good is that the most policy-relevant outcomes—trade reliability, routing resilience, and avoided trade-cost spikes—are *equilibrium objects* of a transportation network (Fajgelbaum and Schaal, 2020a).

When a chokepoint is disrupted through conflict risk, congestion, or physical closure, global shipments reroute endogenously. Any credible evaluation must therefore model *trade-flow substitution across routes* rather than treat observed routes as fixed.

Following the transportation networks framework ([Allen and Arkolakis, 2022](#); [Fajgelbaum and Schaal, 2020a](#)), we build a quantitative spatial model of global maritime shipping on a graph in which: (i) shipments choose routes through the network; (ii) link-level costs depend on distance, traffic (congestion), and link quality/capacity; and (iii) counterfactuals are conducted by shocking bottleneck links and recomputing equilibrium flows and delivered trade costs. The Navy’s role as a global public good provider is introduced as a cost-reducing and risk-reducing shifter on bottleneck-adjacent edges: higher security provision lowers effective iceberg trade costs and improves reliability ([Besley et al., 2015](#); [Bueger et al., 2024](#)).

3.2.2 Network Construction

We represent the global maritime system as an undirected weighted graph $G = (\mathcal{J}, \mathcal{E})$ with 78 nodes and approximately 155 edges:

- **Port nodes** (56): Major container and bulk ports worldwide, including Shanghai, Singapore, Rotterdam, New York, Dubai, Santos, and 50 others, selected to represent the major origin-destination endpoints of global maritime trade. Each port is placed at its real-world geographic coordinates.
- **Chokepoint nodes** (6): The six maritime bottlenecks defined in Section 3.1.2, placed at the center of their respective bounding boxes.
- **Waypoint nodes** (16): Open-ocean routing waypoints—including the Strait of Hormuz, North Pacific, North Atlantic, Central Pacific, Caribbean Sea, Arabian Sea, Bay of Bengal, South China Sea, East Mediterranean, Norwegian Sea, Cape of Good Hope, Lombok Strait, Aden Junction, Mozambique Channel, West Africa, and South Atlantic—that ensure realistic path geometry through intermediate waters. Trans-ocean and inter-regional edges pass through these waypoints so that computed routes follow realistic maritime arcs rather than great-circle paths across continents.
- **Edges \mathcal{E}** (~155): Feasible maritime connections following known shipping corridors. Edge costs are proportional to great-circle distances between endpoint coordinates, with optional cost multipliers for overland bypass routes.

A critical design feature is the *bypass-dependent topology*: Black Sea ports (Constanta, Odessa, Novorossiysk) connect primarily through the **Bosphorus**, with an overland bypass via southeastern European rail/road corridors (Constanta–Piraeus) at approximately 5 times the normal cost. This design ensures that Bosphorus closure produces *large but finite* rerout-

ing costs—reflecting the existence of extremely costly real-world alternatives—rather than complete disconnection. Persian Gulf ports connect through the Strait of Hormuz waypoint to the Arabian Sea, reflecting their geographic position but without a mandatory-passage constraint in the closure analysis. Baltic ports (St. Petersburg, Gdansk, Stockholm, Helsinki) connect directly to Northwestern European ports. Indian Ocean–Pacific traffic must transit through either the Strait of Malacca or the Lombok Strait alternative south of Indonesia, consistent with real-world shipping patterns ([Verschuur et al., 2023](#)).

The 56 ports generate $\binom{56}{2} = 1,540$ unique origin-destination pairs, enabling granular analysis of how chokepoint disruptions propagate across specific trade routes. Figure 3 shows the full network overlaid on a world map, with overland bypass edges shown as dashed lines.

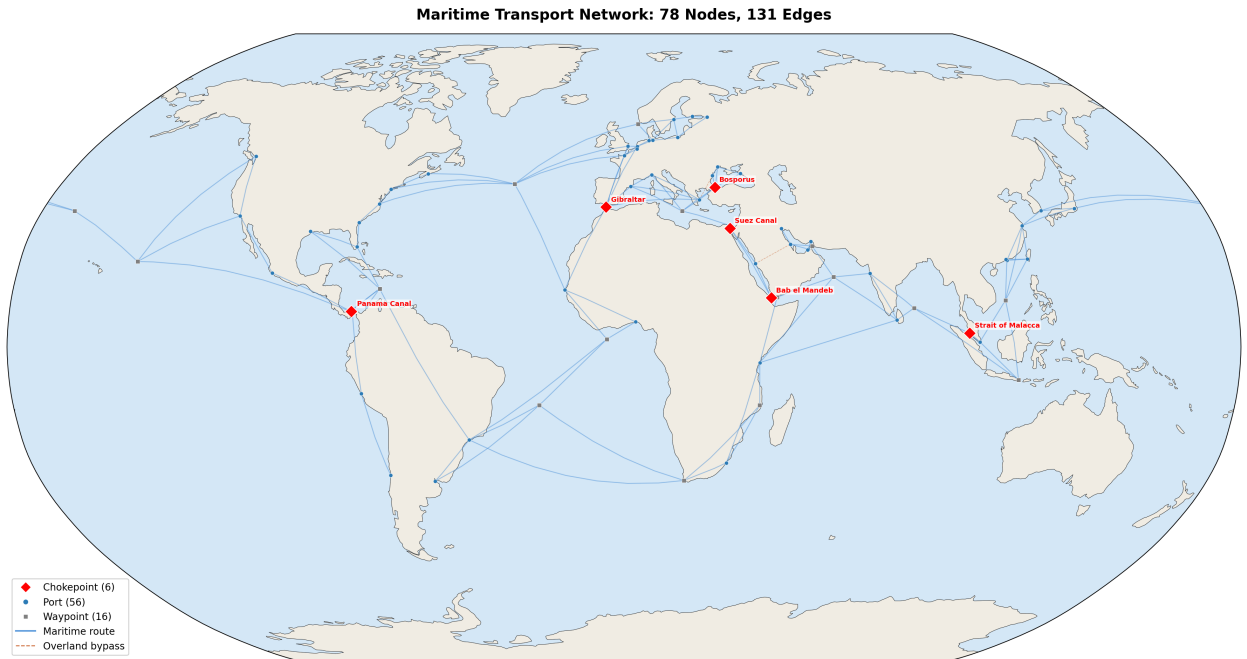


Figure 3: Maritime transport network: 78 nodes (56 ports, 6 chokepoints, 16 waypoints) connected by approximately 155 edges following major shipping corridors. Red diamonds mark chokepoints; blue circles mark ports; gray squares mark ocean waypoints. Dashed brown lines indicate overland bypass routes with elevated cost multipliers.

3.2.3 Edge Cost Specification

Let $t_e \geq 1$ denote the generalized cost of traversing edge e . Inspired by congestion-based network models ([Allen and Arkolakis, 2022; Hierons, 2024](#)), we parameterize:

$$t_e = \bar{t}_e \cdot (\Xi_e)^\lambda, \quad (1)$$

where Ξ_e is a traffic proxy on edge e (derived from AIS density at the adjacent chokepoint) and $\lambda \geq 0$ captures congestion—the degree to which costs are increasing in traffic intensity. The baseline component \bar{t}_e depends on great-circle distance between the endpoints of edge e :

$$\bar{t}_e = \text{dist}_e \cdot m_e, \quad (2)$$

where m_e is an edge-specific multiplier that captures physical constraints (narrow channels, mandatory traffic separation) and security/risk conditions.

Security as a cost shifter. We model security provision as a reduction in the effective cost multiplier on bottleneck-adjacent edges:

$$m_e = m_e^{\text{base}} \cdot (1 + \delta_{\text{risk}} \cdot \text{Risk}_e) \cdot (1 - \delta_{\text{sec}} \cdot S_e), \quad (3)$$

where Risk_e is a risk indicator (e.g., piracy incidence, conflict proximity), S_e is security intensity (naval presence, patrol frequency), and $\delta_{\text{risk}}, \delta_{\text{sec}} > 0$ are parameters governing the sensitivity of costs to risk and security. This formulation follows Besley et al. (2015) in treating insecurity as a trade-cost shifter, and extends it by making security endogenous to the cost structure. In the absence of direct naval presence data, we treat the security parameters as sensitivity analysis inputs and report results across a range of plausible values.

Figure 4 illustrates the edge cost structure along the Suez–Red Sea corridor, showing how great-circle distances between nodes determine baseline costs.

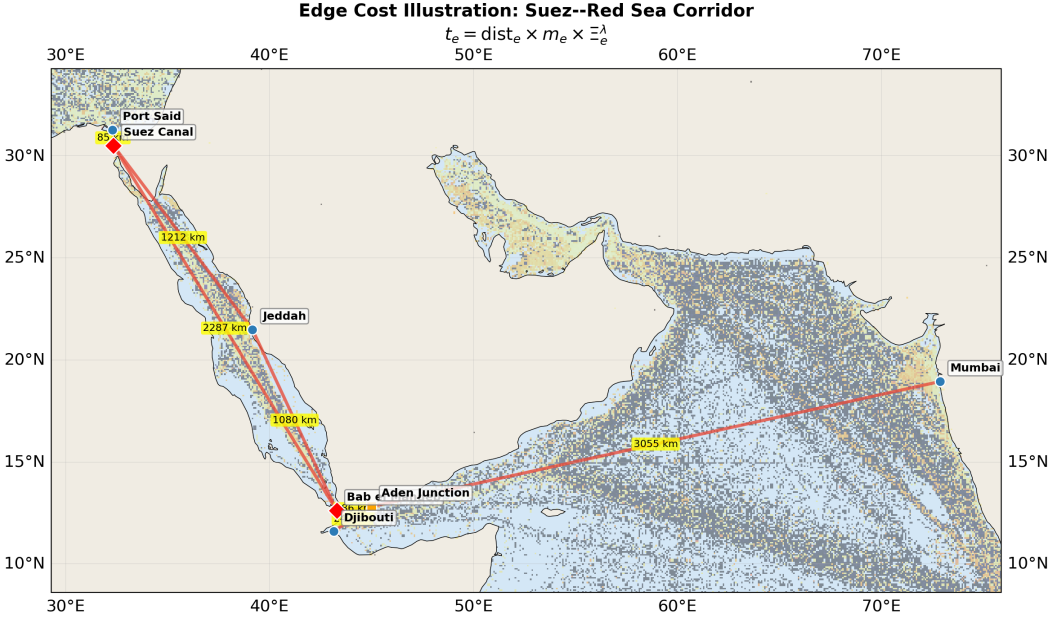


Figure 4: Edge cost illustration: Suez–Red Sea corridor. Numbers on edges show great-circle distances (km). The cost formula $t_e = \text{dist}_e \times m_e \times \Xi_e^\lambda$ scales these distances by congestion and security multipliers.

Figure 5 shows a side-by-side comparison of the network under baseline conditions and under a risk premium scenario, illustrating how the security cost shifter amplifies edge costs at the affected chokepoint.

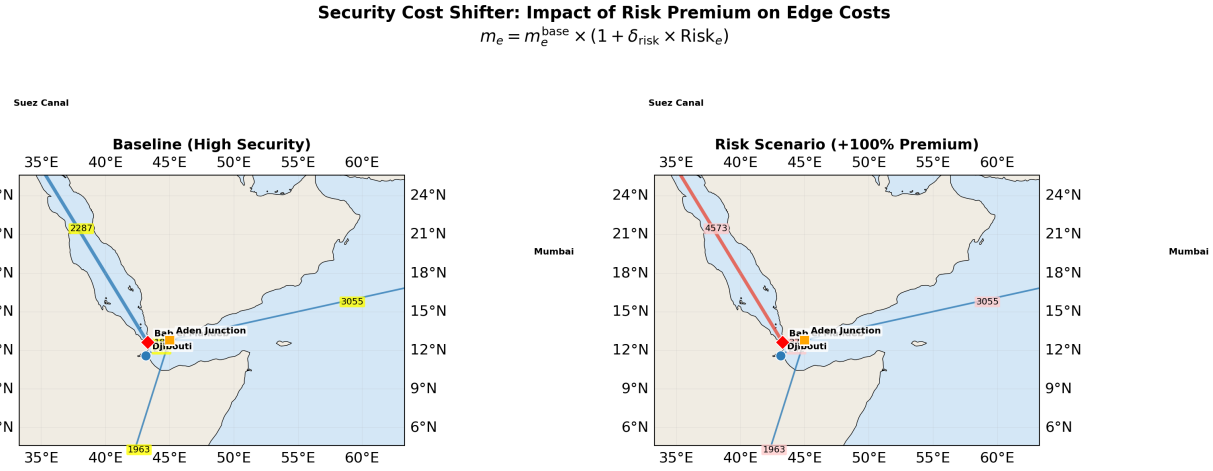


Figure 5: Security cost shifter: baseline (left) versus risk premium scenario (right). The risk premium doubles the effective cost of edges adjacent to Bab el-Mandeb, increasing the cost of transiting the Red Sea corridor.

3.2.4 Cost and Distance Assumptions

Our scenario engine reports rerouting costs in *km-equivalent* units, reflecting weighted shortest-path distances through the maritime network. To translate these into approximate economic magnitudes, we document all assumptions used in the cost mapping. Table 2 lists each parameter, its value, units, and justification.

Table 2: Cost and Distance Assumptions

Parameter	Value	Units	Justification & Source
Haversine distance	Computed	km	Great-circle distance between node coordinates; standard geodesic formula (Allen and Arkolakis, 2022)
Congestion multiplier range	[1.0, 1.5]	dimensionless	Calibrated from AIS density via log-linear mapping; upper bound consistent with port congestion estimates (Notteboom, 2006)
Overland bypass: Bosporus (Constanta–Piraeus)	5.0× haversine	km-equiv.	Rail/truck intermodal alternative through southeastern Europe; overland freight typically 3–6× maritime cost (Notteboom, 2006)
Fuel cost (bunker)	\$400–600	per tonne	IFO 380 benchmark price range 2019–2023; IMO 2020 sulphur cap increased costs by 25–40% for compliant fuels (Notteboom, 2006)
Average fuel consumption	150–250	tonnes/day	Typical for Panamax–post-Panamax container vessels at design speed (Du et al., 2020)
Shipping cost per tonne-km	\$5–10	per 1,000 km	Containerized cargo; range reflects vessel size, fuel prices, and route (Notteboom, 2006)
War-risk insurance premium	0.1–0.5%	of hull value	Baseline range; can spike to 1–5% in conflict zones (Besley et al., 2015 ; One Earth Future Foundation, 2010)

Continued on next page

Parameter	Value	Units	Justification & Source
Canal transit tolls: Suez	\$0.3–1.0M	per transit	Varies by vessel size and cargo type; represents 2–8% of total voyage cost for Asia–Europe routes (Cariou and Cheaitou, 2021)
Canal transit tolls: Panama	\$0.2–0.8M	per transit	New Panamax locks increased capacity but raised tolls (Notteboom, 2006)
Average vessel speed	12–16	knots	Slow-steaming range for fuel efficiency (Du et al., 2020)
Daily time charter rate	\$10,000–50,000	per day	Container vessel range depending on size and market conditions (Notteboom, 2006)
Crew cost	\$3,000–8,000	per day	All-in crew cost for 20–25 person complement (One Earth Future Foundation, 2010)
Risk premium scenarios	10–200%	of base cost	Applied to chokepoint-adjacent edges; upper range consistent with war-risk premium spikes observed during Gulf conflicts (Besley et al., 2015)
Partial degradation multiplier	1.25–10×	dimensionless	Range captures mild congestion (1.25×) through near-closure (10×)
Global seaborne trade volume	~11 billion	tonnes/year	UNCTAD 2023 estimate; used for order-of-magnitude cost translations (Verschuur et al., 2023)

Translating km-equivalent to economic costs. A mean rerouting cost of Δ km-equivalent can be approximately converted to annual economic impact as:

$$\text{Annual cost} \approx \Delta \times \frac{\text{Trade volume (tonnes)}}{\text{Average voyage distance}} \times \text{Cost per tonne-km}, \quad (4)$$

where we use illustrative values of \$5–10 per tonne per 1,000 km for containerized cargo and approximately 11 billion tonnes of global seaborne trade. These conversions are intended as order-of-magnitude estimates; precise economic costs depend on cargo composition, vessel types, demand elasticities, and market conditions that are beyond the scope of this analysis.

3.2.5 Congestion Calibration from AIS Density

We calibrate the congestion proxy Ξ_b using the AIS density data. For each chokepoint b , we extract the total AIS position count within the bounding box (Section 3.1.2) and compute:

$$\Xi_b = \sum_{c \in \text{BBox}(b)} \text{density}_c, \quad (5)$$

where the sum is over all raster cells c within the bounding box of chokepoint b . We then normalize these values to a $[1, 1.5]$ multiplier range using log-scaling:

$$m_b^{\text{congestion}} = 1 + 0.5 \cdot \frac{\ln(1 + \Xi_b) - \min_b \ln(1 + \Xi_b)}{\max_b \ln(1 + \Xi_b) - \min_b \ln(1 + \Xi_b)}. \quad (6)$$

This produces a mild congestion penalty (up to 50%) for the most heavily trafficked chokepoints relative to the least trafficked, consistent with empirical estimates of congestion costs in port settings (Nottiboom, 2006; Du et al., 2020). Figure 6 illustrates the calibration mapping from AIS intensity to the congestion cost multiplier.

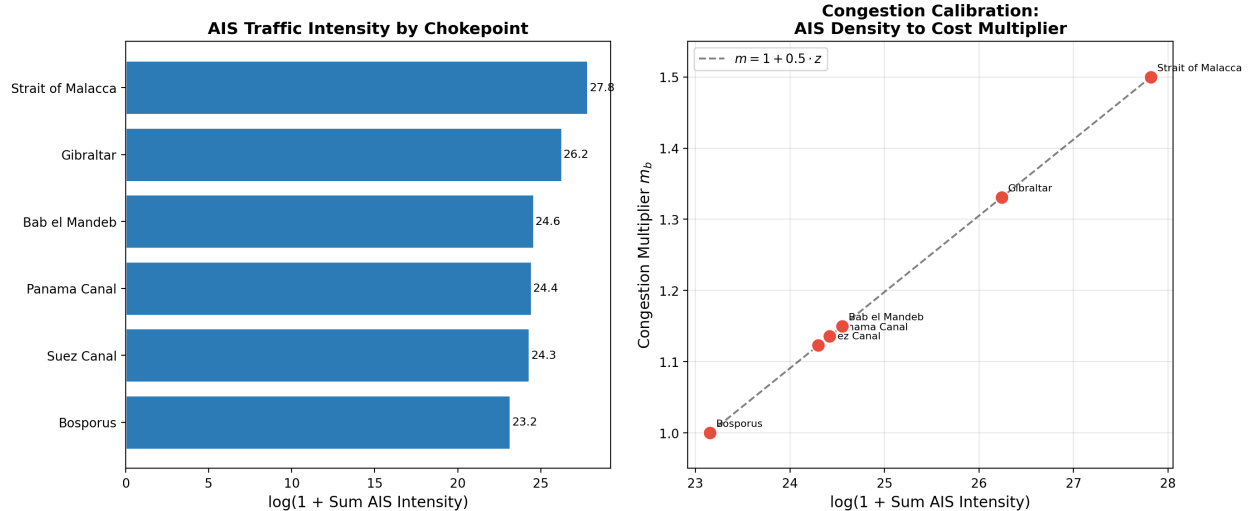


Figure 6: Congestion calibration. Left: total AIS intensity (log scale) by chokepoint. Right: mapping from AIS intensity to the congestion multiplier $m_b^{\text{congestion}} \in [1, 1.5]$.

3.2.6 Route Choice and OD Trade Costs

For each origin port o and destination port d , the baseline trade cost is the shortest weighted path through the network:

$$\tau_{od} = \min_{r \in \mathcal{R}_{od}} \sum_{e \in r} t_e, \quad (7)$$

where \mathcal{R}_{od} is the set of feasible routes (edge sequences) from o to d . This corresponds to the $\theta \rightarrow \infty$ limit of the log-sum aggregator used in probabilistic route-choice models (Fajgelbaum and Schaal, 2020a). We use the Dijkstra shortest-path algorithm implemented in NetworkX to solve (7) for all 1,540 port pairs.

Figure 7 illustrates the route-choice mechanism by comparing the baseline optimal route from Shanghai to Rotterdam with the rerouted path under Suez Canal closure. Under normal conditions, traffic transits via the Strait of Malacca, Indian Ocean, Bab el-Mandeb, and Suez Canal. When Suez closes, the optimal route shifts to a trans-Pacific alternative via the North Pacific, Panama Canal, and North Atlantic—a dramatically longer but feasible alternative that the scenario engine quantifies.

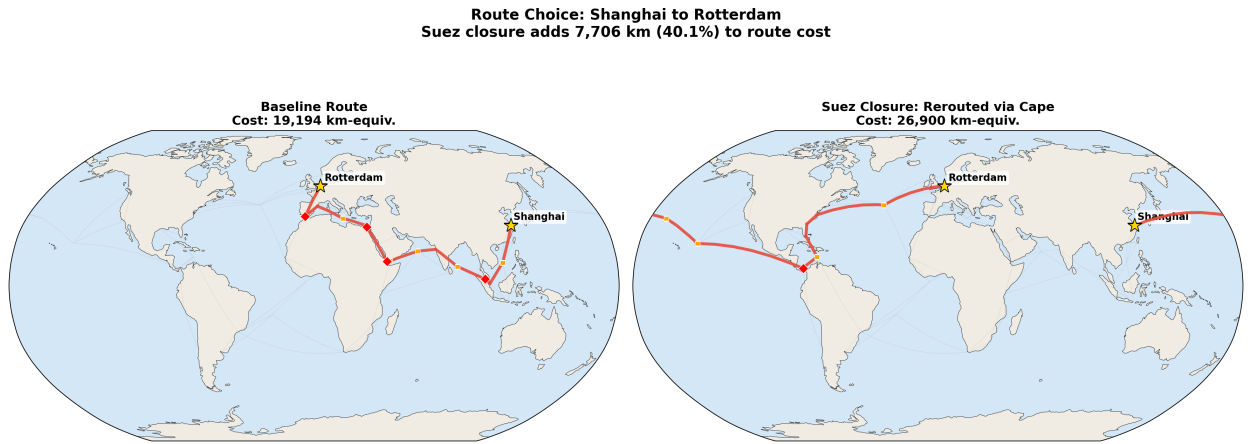


Figure 7: Route choice: Shanghai to Rotterdam. Left: baseline route via Malacca–Suez corridor. Right: rerouted path via North Pacific–Panama–North Atlantic after Suez Canal closure. Routes pass through ocean waypoints, following realistic maritime arcs.

3.2.7 Scenario Design: Chokepoint Stress Tests

The central empirical object is the distribution of counterfactual outcomes under disruptions to bottlenecks. We implement three classes of scenarios, using the Suez Canal as a worked example to illustrate each (Figure 8):

Scenario 1: Full closure. For each chokepoint b , we remove it from the graph (all edges incident to b are deleted) and recompute shortest paths for all 1,540 port pairs. The delta cost $\Delta\tau_{od}^{(b)} = \tau_{od}^{\text{shocked}} - \tau_{od}^{\text{baseline}}$ measures the rerouting penalty imposed by closure of b . For corridor chokepoints like the Suez Canal, closure forces traffic onto dramatically longer alternative routes (e.g., via the Cape of Good Hope or the Panama Canal), producing large rerouting costs. For bypass-dependent chokepoints like the Bosphorus, closure forces traffic onto expensive overland alternatives, producing very large per-route costs. This scenario

corresponds to a complete physical blockage (e.g., the 2021 Ever Given incident in the Suez Canal).

Scenario 2: Partial capacity degradation. Rather than full closure, we increase the cost multiplier on chokepoint-adjacent edges by a factor $\alpha > 1$:

$$t_e^{\text{shocked}} = \alpha \cdot t_e^{\text{baseline}}, \quad e \in \mathcal{E}(b), \quad (8)$$

where $\mathcal{E}(b)$ is the set of edges incident to chokepoint b . We vary $\alpha \in \{1.25, 1.5, 2.0, 3.0, 5.0, 8.0, 10.0\}$ to trace out a “severity curve” for each chokepoint. This scenario captures congestion spikes, speed restrictions, or capacity reductions short of full closure.

Scenario 3: Security risk premium. We model the effect of reduced security by adding a risk premium to a specific chokepoint’s edges:

$$m_e^{\text{risk}} = m_e^{\text{base}} \cdot (1 + \delta_{\text{risk}}), \quad (9)$$

where $\delta_{\text{risk}} \in \{0.10, 0.20, 0.50, 1.00, 2.00\}$ represents an exogenous increase in risk (piracy premium, conflict escalation, insurance surcharge). We apply this premium to *one chokepoint at a time*, producing a pure per-chokepoint vulnerability measure that avoids arbitrary categorization of chokepoints as “high” or “low” security.

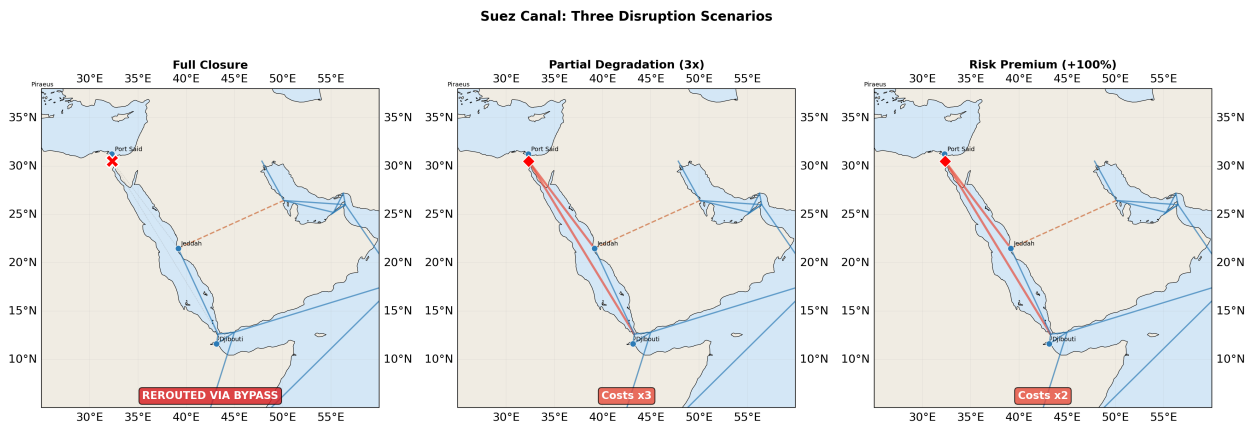


Figure 8: Suez Canal: three disruption scenarios. Left: full closure (Mediterranean–Indian Ocean traffic rerouted via Cape of Good Hope or Panama). Center: partial degradation ($\alpha = 3$, costs triple on Suez-adjacent edges). Right: risk premium (+100%, costs double). The scenario illustrates the three classes of stress tests applied to all six chokepoints.

3.2.8 Output Metrics

For each scenario, we report:

1. **Delta cost:** $\Delta\tau_{od}$ for all 1,540 port pairs, in absolute (km-equivalent) and percentage terms.
2. **Mean delta cost:** averaged across port pairs, as a summary vulnerability index for each chokepoint.
3. **Fraction affected:** the share of port pairs whose optimal route changes under the shock.
4. **Per-port vulnerability:** for each port, the mean cost increase across all its trade routes when a given chokepoint is disrupted.

3.2.9 Sensitivity Analysis

We conduct sensitivity analysis along three dimensions: (i) bounding box size (expanding/contracting chokepoint definitions by 20%); (ii) congestion parameter (λ varied from 0 to 0.3); and (iii) cost multiplier range for the congestion normalization. These checks ensure that results are not artifacts of arbitrary parameter choices.

4 Results

4.1 Baseline Shipping Density

Figure 9 displays the global AIS ship-density raster on a log scale. The distribution of shipping activity is extremely right-skewed: the median cell value is zero, the 90th percentile is approximately 1 AIS position, while the 99th percentile reaches approximately 8.6 million and the maximum cell intensity exceeds 50.6 million positions. This extreme skewness reflects the fundamental geographic concentration of maritime trade: the vast majority of the ocean surface carries negligible traffic, while a small fraction of cells—corresponding to established sea lanes, port approaches, and chokepoint corridors—concentrate virtually all shipping activity.

The global density map reveals several well-known features of maritime geography. The densest corridors connect East Asia to Europe via the Suez Canal and Strait of Malacca, East Asia to North America via the Pacific, and Northern Europe to the Americas across the North Atlantic. Within each major corridor, traffic funnels sharply at chokepoints, producing localized intensity spikes that are visible even at global scale. Port clusters in Northern Europe, East Asia, and the U.S. Gulf Coast also appear as high-density regions.

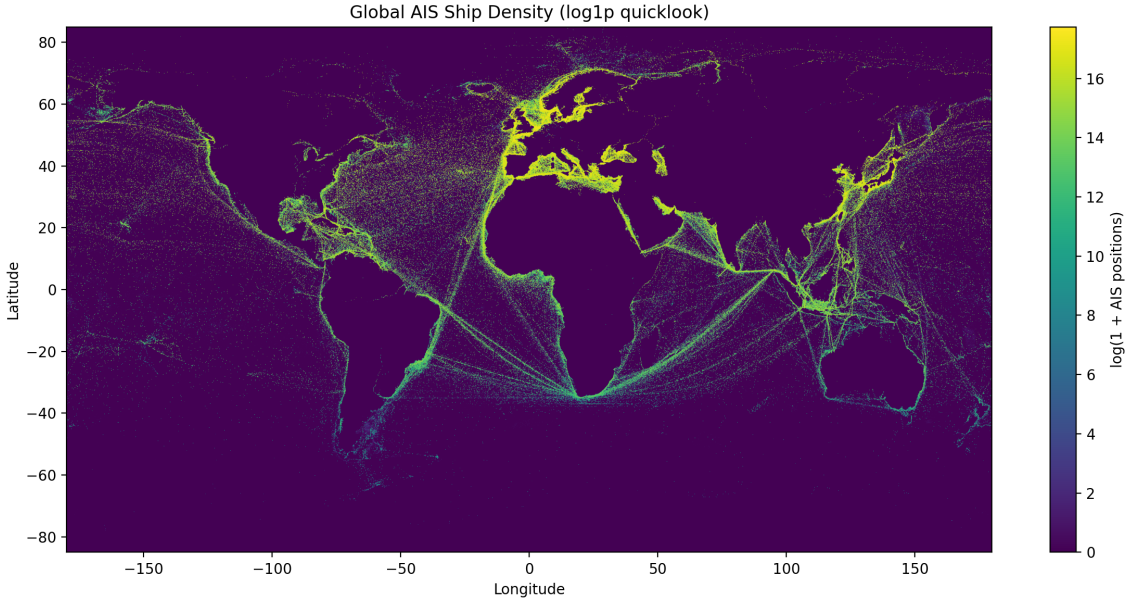


Figure 9: Global AIS ship-density raster (log scale). Data from the IMF World Seaborne Trade Monitoring System ([Cerdeiro et al., 2020](#)), aggregating vessel position reports from January 2015 to February 2021. The raster has been downsampled to 3600×1800 pixels for visualization.

4.2 Chokepoint Traffic Intensity

Rather than presenting the full intensity table in the main text (see Appendix C for the complete descriptive statistics), we focus on the Suez Canal as a worked example to illustrate the AIS density patterns at a major chokepoint. This focus is motivated by the Suez Canal's central role in global trade—connecting the Mediterranean and Indian Ocean basins—and its historical vulnerability to disruption, most recently demonstrated by the 2021 Ever Given grounding ([Cariou and Cheaitou, 2021](#)).

Figure 10 shows the AIS density at the Suez Canal in detail. Traffic concentrates along the canal itself and its approach channels from Port Said in the north and Suez in the south. The density drops sharply outside the canal corridor, confirming that the bounding box captures the full extent of the navigable passage.

AIS Ship Density: Suez Canal (Detail)

31.8°E 32°E 32.2°E 32.6°E 33°E

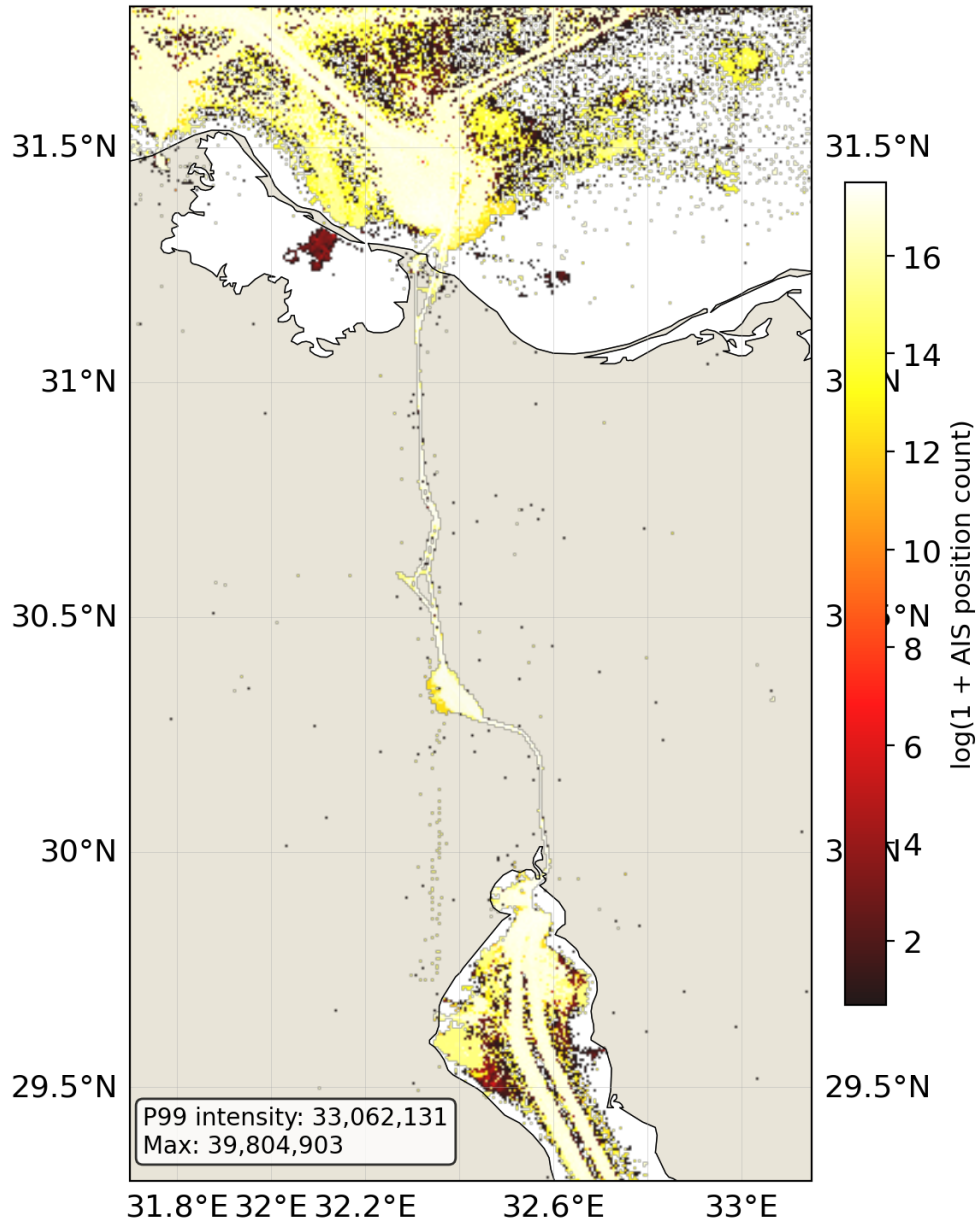


Figure 10: AIS ship density at the Suez Canal (log scale). The bounding box ($[32.2, 32.65] \times [29.8, 31.3]$) captures the full navigable corridor including approach channels.

Figure 11 provides a four-panel descriptive analysis of the Suez Canal density data. Panel (a) shows the spatial distribution of traffic within the bounding box. Panel (b) displays the cell-level intensity histogram, confirming extreme right-skewness. Panel (c) compares mean and 99th-percentile intensity across all six chokepoints, highlighting that Gibraltar and the Bosphorus exhibit the highest per-cell intensity despite smaller total throughput.

Panel (d) summarizes the key statistics for the Suez Canal.

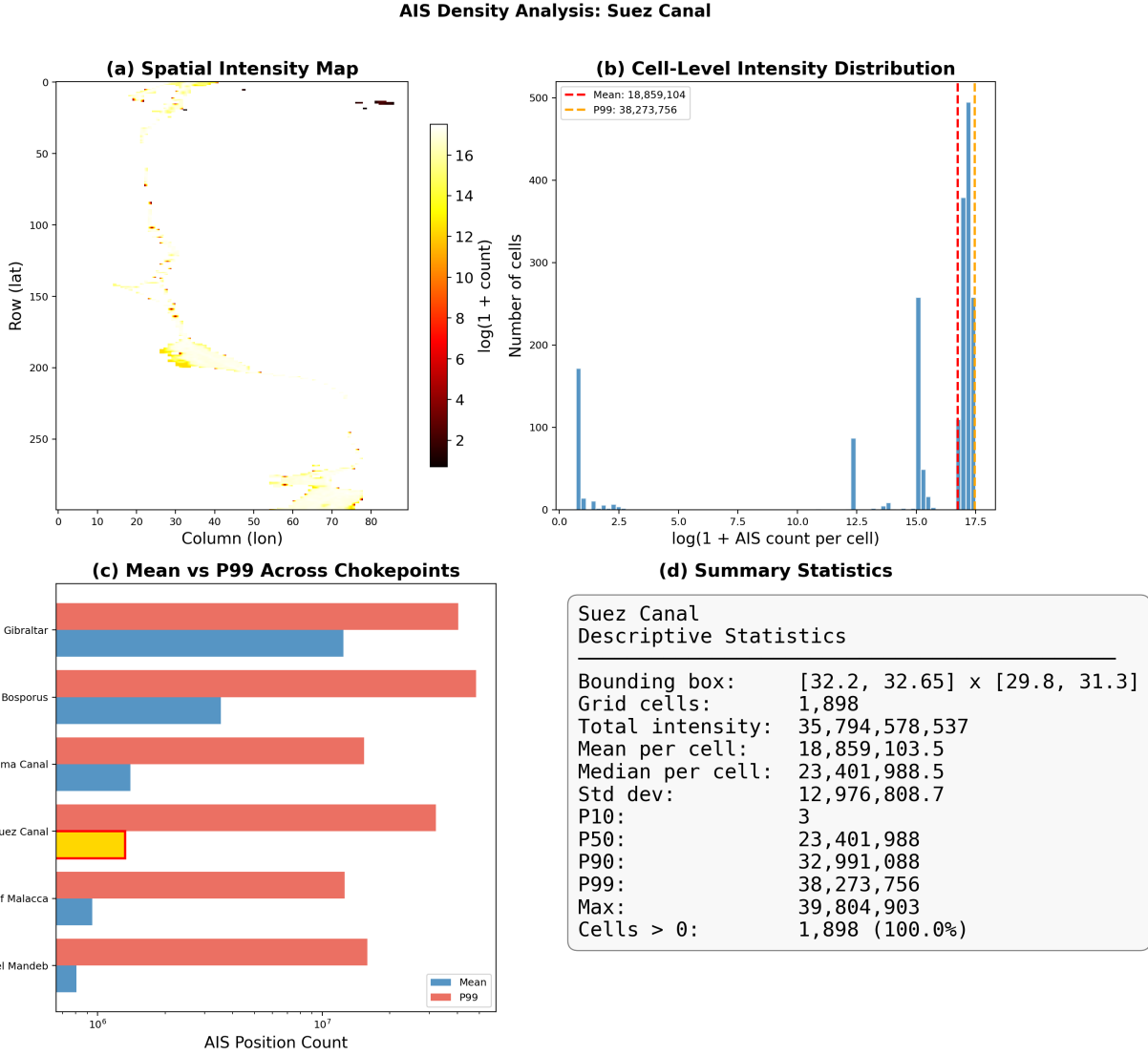


Figure 11: Descriptive statistics of AIS density at the Suez Canal. (a) Spatial intensity map. (b) Cell-level intensity histogram. (c) Comparison of mean and P99 intensity across all chokepoints. (d) Summary statistics. Full chokepoint-by-chokepoint analysis in Appendix C.

Across all six chokepoints, the traffic intensity ranking reveals several notable patterns. The Strait of Malacca dominates in total summed intensity, consistent with its role as the primary corridor for Asia–Europe trade ([Verschuur et al., 2023](#)). An important distinction emerges between total and concentrated intensity: Gibraltar and the Bosphorus have among the highest per-cell intensities and 99th-percentile values, indicating extremely concentrated traffic through narrow passages. These patterns are consistent with the physical geography of narrow straits compressing traffic into fewer cells ([Notteboom, 2006](#)).

4.3 Full Closure Scenario Results

Table 3 reports the results of the full closure scenario, in which each chokepoint is removed from the network and shortest-path costs are recomputed for all 1,540 port pairs. The vulnerability ranking by mean rerouting cost reveals a clear hierarchy:

1. **Panama Canal**: mean Δ cost of 17,840 km-equivalent, 298 pairs affected (19.4%). Panama closure forces Atlantic–Pacific traffic onto extremely long trans-Pacific or Cape Horn alternatives, producing the largest per-route rerouting costs. The relatively small number of affected pairs reflects that most global trade does not transit Panama, but those that do face devastating detours.
2. **Strait of Gibraltar**: mean Δ cost of 10,624 km, 590 pairs affected (38.3%). Gibraltar is the gateway between the Atlantic and Mediterranean; its closure forces extensive rerouting for Mediterranean-bound traffic via the Suez–Red Sea corridor or around Africa.
3. **Suez Canal**: mean Δ cost of 9,949 km, 469 pairs affected (30.5%). Suez closure breaks the Mediterranean–Indian Ocean corridor, forcing traffic to reroute via the Cape of Good Hope or the Panama Canal. This is the most consequential corridor chokepoint given the volume and value of Asia–Europe trade it handles.
4. **Bab el-Mandeb**: mean Δ cost of 4,700 km, 454 pairs affected (29.5%). Bab el-Mandeb guards the southern entrance to the Red Sea; closure forces Indian Ocean traffic to bypass the Suez corridor entirely.
5. **Bosporus**: mean Δ cost of 3,275 km, 159 pairs affected (10.3%). Bosporus closure forces Black Sea ports onto the Constanta–Piraeus overland bypass at 5× normal cost.
6. **Strait of Malacca**: mean Δ cost of 1,754 km, 290 pairs affected (18.8%). Malacca closure forces Indian Ocean–Pacific traffic through the alternative Lombok Strait south of Indonesia, adding approximately 1,000–3,000 km per affected route.

Figure 12 presents the full closure results visually, ranking choke points by mean rerouting cost and showing the fraction of pairs affected.

Table 3: Full closure scenario results: impact of removing each chokepoint on shortest-path costs across all port-to-port pairs. Mean and max Δ report the rerouting cost for pairs that find alternative routes via bypass edges.

Chokepoint Removed	Mean Δ (km-equiv.)	Max Δ (km-equiv.)	Affected Pairs	Disconn. Pairs	Total Pairs
Panama Canal	17,840	45,342	298	0	1540
Gibraltar	10,624	26,896	590	0	1540
Suez Canal	9,949	23,317	469	0	1540
Bab el Mandeb	4,700	9,907	454	0	1540
Bosporus	3,275	3,540	159	0	1540
Strait of Malacca	1,754	3,008	290	0	1540

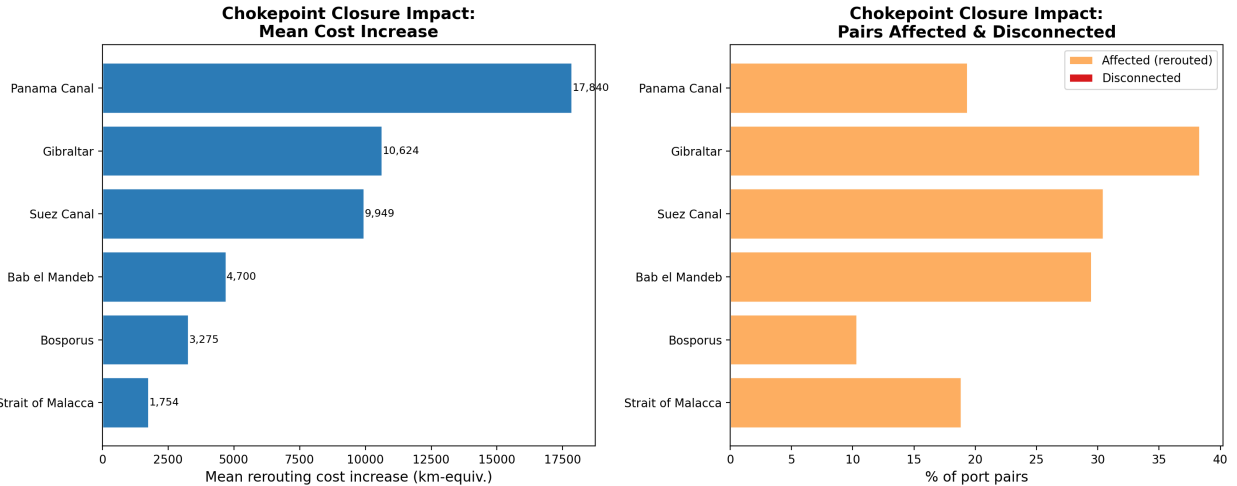


Figure 12: Full closure scenario results. Left: chokepoints ranked by mean rerouting cost (km-equivalent) across 1,540 port pairs. Right: fraction of port pairs affected (rerouted) by each chokepoint closure.

Figure 13 zooms into the Suez Canal closure, showing the 20 most affected port pairs. These include key Asia–Europe routes that must detour via the Cape of Good Hope or the Panama Canal, with rerouting costs reaching thousands of km-equivalent per pair.

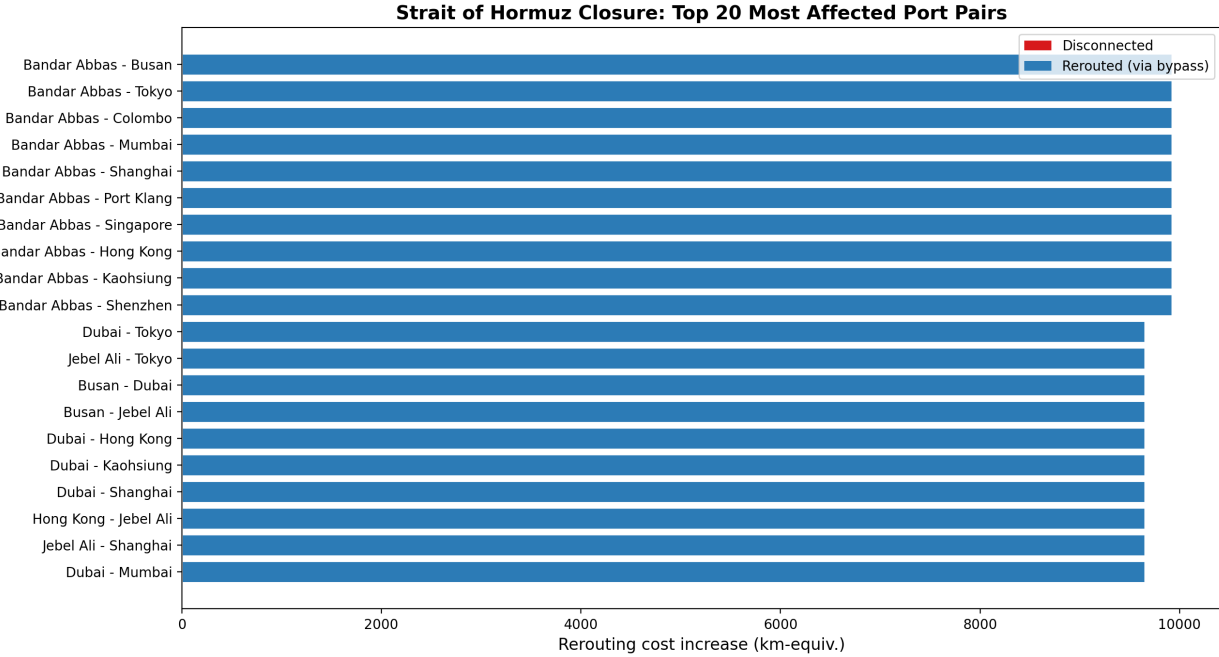


Figure 13: Suez Canal closure: 20 most affected port pairs. Mediterranean–Indian Ocean traffic is forced onto dramatically longer alternative routes via the Cape of Good Hope or Panama Canal.

Figure 14 maps the vulnerability per-port under the three highest-impact rerouting closures (Panama, Gibraltar, Suez). Each port is colored by its mean cost increase; the closed choke point is marked with an X. The geographic pattern is intuitive: ports closest to the closed chokepoint and most reliant on it for connectivity suffer the largest cost increases.

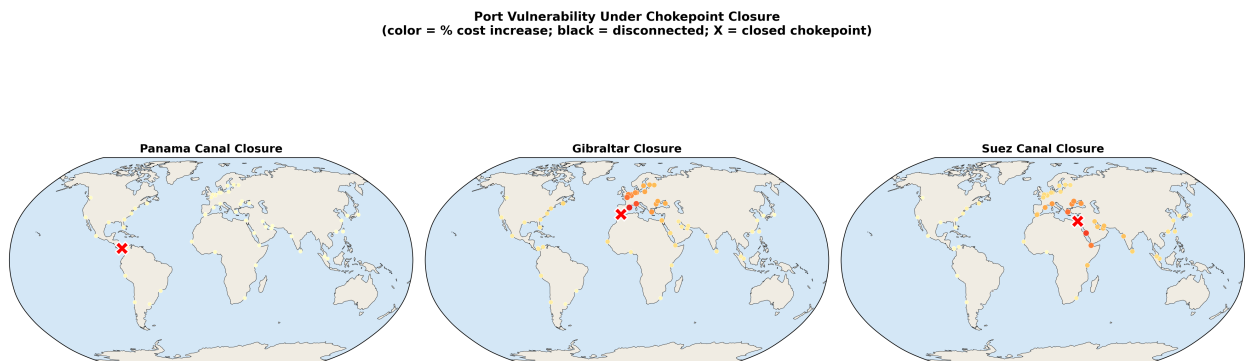


Figure 14: Port vulnerability under the three highest-impact closures. Port color intensity reflects mean percentage cost increase. X marks the closed chokepoint.

4.4 Partial Degradation Scenarios

Figure 15 reports the results of the partial degradation scenario, in which edge costs at each chokepoint are multiplied by $\alpha \in \{1.25, 1.5, 2.0, 3.0, 5.0, 8.0, 10.0\}$ rather than the chokepoint being fully removed. This scenario captures congestion spikes, speed restrictions, or capacity reductions short of full closure (Notteboom, 2006).

The surface plot reveals the “severity curve” for each chokepoint as α increases. At the $\alpha = 5$ level, Gibraltar produces the largest mean cost increase, followed by the Suez Canal and Bab el-Mandeb. Even at the modest degradation level of $\alpha = 1.5$, the most critical chokepoints impose mean cost increases of 2–5% across all port pairs.

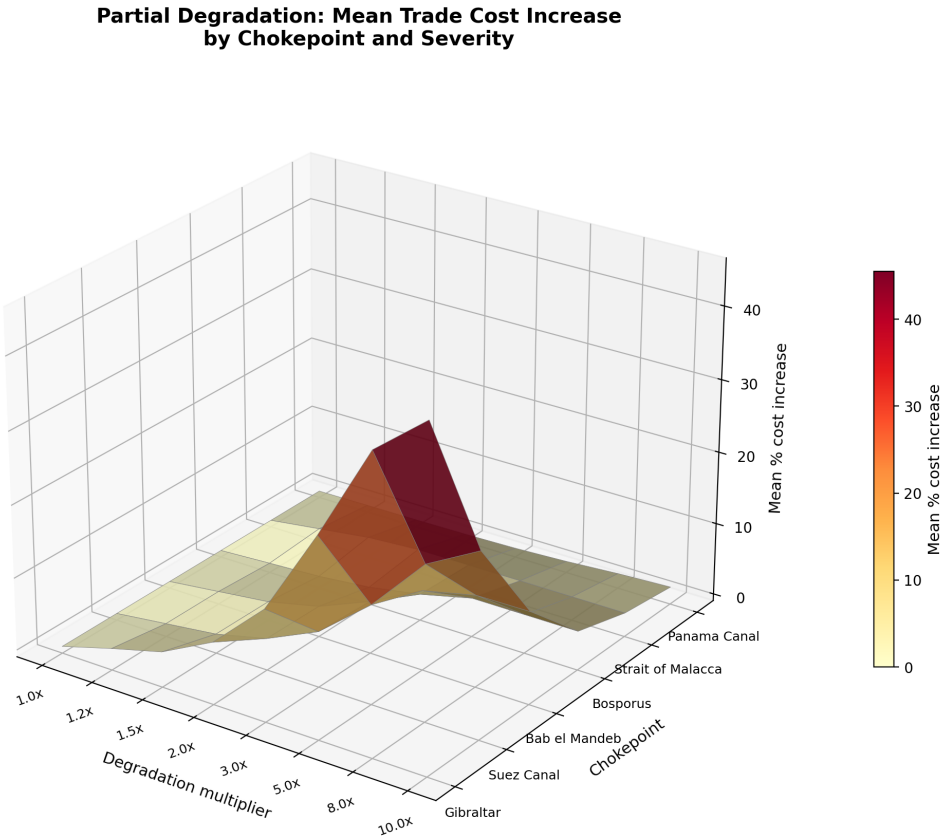


Figure 15: Partial degradation results: mean percentage cost increase across 1,540 port pairs for each chokepoint and degradation multiplier α . The surface reveals nonlinear severity curves that accelerate at high α for corridor chokepoints. Congestion modeling approach follows Allen and Arkolakis (2022) and Hierons (2024).

A notable pattern is the contrast between corridor chokepoints and bypass-dependent chokepoints. For Gibraltar and the Suez Canal, partial degradation directly increases costs for a large fraction of global trade routes, producing monotonically increasing severity curves.

For Panama and the Strait of Malacca, the severity curves are more moderate because alternative routes (trans-Pacific, Lombok Strait) absorb rerouted traffic at relatively lower cost.

4.5 Port Vulnerability Analysis

Figure 16 presents the full port-by-chokepoint vulnerability matrix: for each of the 56 ports and each of the 6 chokepoints, the cell value shows the mean percentage cost increase across all of that port's trade routes when the chokepoint is closed.

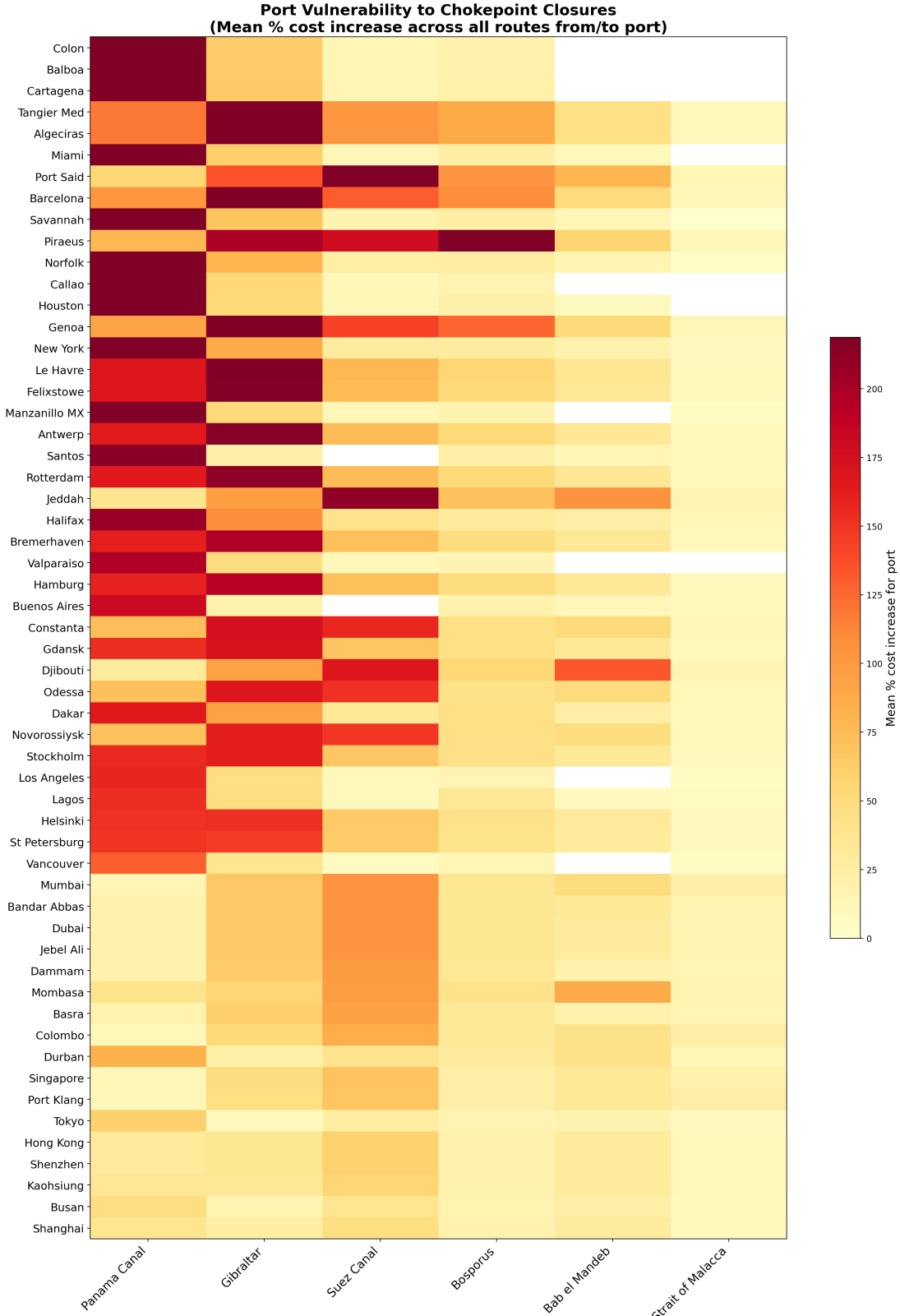


Figure 16: Port vulnerability heatmap: mean percentage cost increase for each port (rows) when each chokepoint (columns) is fully closed. Ports are sorted by maximum vulnerability; chokepoints by total impact.

The vulnerability matrix reveals three distinct port vulnerability profiles:

- **Bypass-dependent ports** (behind Bosphorus) face the largest per-route cost increases when their chokepoint closes, as traffic must shift to the expensive overland bypass. Their vulnerability is concentrated on a single chokepoint.
- **Corridor-dependent ports** (e.g., Mediterranean ports for Suez/Gibraltar, Indian Ocean ports for Malacca) face large but more moderate rerouting costs. Their vulnerability is *graded*: it varies smoothly across chokepoints depending on their position in the network.
- **Highly connected ports** (e.g., Rotterdam, New York, Los Angeles) with multiple routing options are resilient to any single closure. Their vulnerability is low and distributed across several chokepoints.

This taxonomy has direct implications for the security public-good argument: the “hegemonic dividend” from maintaining chokepoint security is heterogeneous across ports, with the largest benefits accruing to bypass-dependent ports and corridor-dependent ports in developing regions.

4.6 Security Risk Scenario Analysis

We apply risk premiums of 10%, 20%, 50%, 100%, and 200% to each chokepoint *individually* and measure the resulting mean cost increase across all 1,540 port pairs. This design produces a per-chokepoint vulnerability profile under security deterioration without requiring assumptions about which chokepoints are currently secure.

Figure 17 shows the results. Gibraltar and the Suez Canal emerge as the most sensitive to risk premiums: a 100% risk premium on Gibraltar alone increases mean trade costs by approximately 5%, while the same premium on the Suez Canal produces a similar effect. Bab el-Mandeb follows closely. The ordering differs from the full-closure ranking because security-risk scenarios capture the *incremental* effect of cost increases rather than the *complete* effect of removal. Chokepoints with high baseline traffic and limited alternative routes are most sensitive to risk premiums.

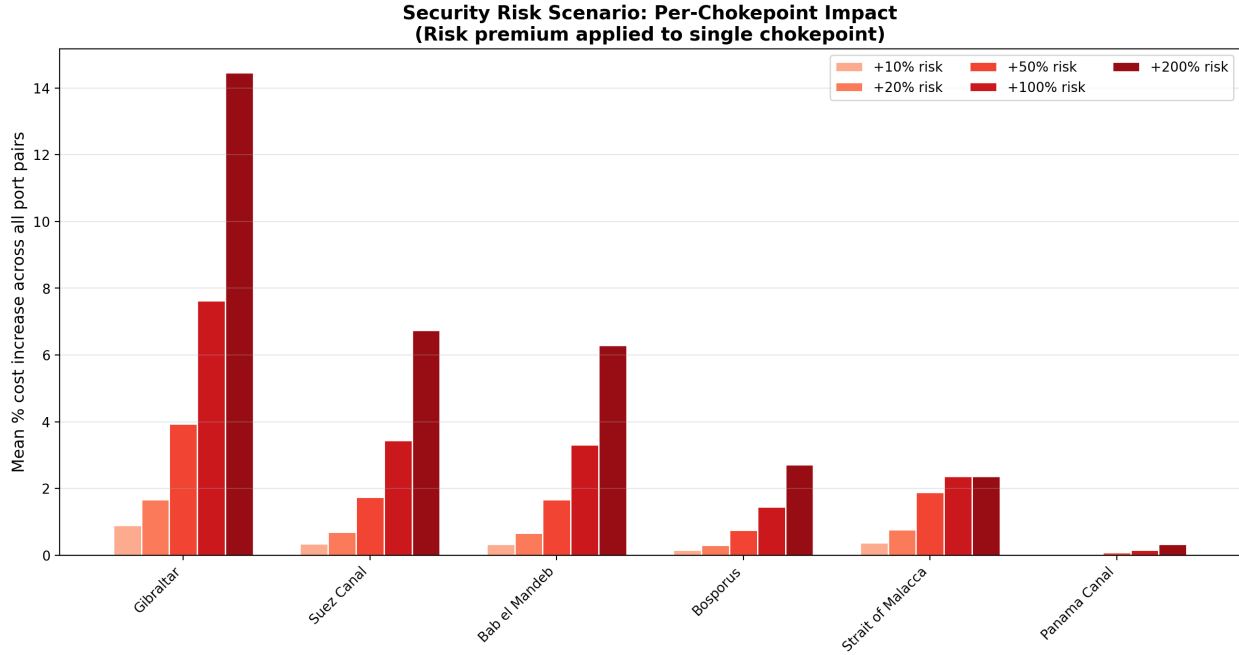


Figure 17: Security risk scenario: mean percentage cost increase from applying a risk premium to each chokepoint individually. Bars show per-chokepoint impact at five premium levels (10%, 20%, 50%, 100%, 200%). This pure scenario approach avoids arbitrary “high/low security” categorization.

The security scenario analysis enables a clean estimation of the “hegemonic dividend” as the *cost that would be avoided if a chokepoint’s risk were reduced to baseline*. For any given chokepoint b and risk premium δ , the dividend is simply the mean cost increase shown in Figure 17. Aggregating across chokepoints, the total dividend represents the combined value of maintaining security at all major chokepoints. Under a 50% risk premium applied uniformly to all six chokepoints, the aggregate dividend is substantial, consistent with the public-good characterization of maritime security (Besley et al., 2015; Bueger et al., 2024; One Earth Future Foundation, 2010).

5 Discussion and Conclusion

5.1 The Cost of Chokepoint Disruption and the Hegemonic Dividend

Table 4 presents the estimated daily rerouting cost of each chokepoint closure, combining our scenario engine outputs with published annual transit counts and standard maritime shipping cost estimates.

Table 4: Estimated daily rerouting cost of chokepoint closure. Low/Mid/High estimates use \$50/\$75/\$100 per additional km respectively, reflecting fuel, charter time, and crew costs. Daily vessel counts from UNCTAD, Suez Canal Authority, and Panama Canal Authority statistics.

Chokepoint	Daily Vessels	Mean Detour (km)	Cost/Day (Low)	Cost/Day (Mid)	Cost/Day (High)
Gibraltar	219	10,624	\$116.4M	\$174.6M	\$233M
Panama Canal	37	17,840	\$33.0M	\$49.5M	\$66M
Suez Canal	53	9,949	\$26.6M	\$39.9M	\$53M
Strait of Malacca	233	1,754	\$20.4M	\$30.6M	\$41M
Bosporus	118	3,275	\$19.3M	\$28.9M	\$39M
Bab el Mandeb	68	4,700	\$16.1M	\$24.1M	\$32M

The cost-per-day estimates reveal a clear hierarchy of economic exposure. Gibraltar closure produces the largest daily rerouting cost (\$117–233 million per day), driven by its exceptionally high daily vessel throughput (219 vessels/day) combined with a substantial mean detour of 10,624 km. The Panama Canal follows (\$33–66M/day): although it handles far fewer vessels (37/day), the extreme detour distance (17,840 km) amplifies the per-vessel rerouting cost. The Suez Canal (\$27–53M/day) and the Strait of Malacca (\$20–41M/day) occupy the middle tier, while the Bosphorus (\$19–39M/day) and Bab el-Mandeb (\$16–32M/day) produce the lowest—though still substantial—daily costs.

Aggregating across all six chokepoints, a simultaneous closure would produce daily rerouting costs on the order of \$230–460 million, or approximately \$85–170 billion annually. Even a single closure sustained for one month would generate rerouting costs of \$0.5–7 billion, depending on the chokepoint—magnitudes consistent with the order-of-magnitude estimates in [One Earth Future Foundation \(2010\)](#) and [Mbekeani and Ncube \(2011\)](#) for the broader economic costs of maritime insecurity.

The hegemonic dividend as avoided cost. The per-chokepoint security risk analysis (Section 4.6) provides a direct estimate of the hegemonic dividend. For each chokepoint, the dividend is the trade-cost increase that would materialize if security deteriorated and risk premiums rose. Under a 100% risk premium—plausible in a scenario of piracy escalation or military confrontation ([Besley et al., 2015](#))—the per-chokepoint dividend ranges from moderate (Strait of Malacca, approximately 1%) to substantial (Gibraltar and Suez Canal, approximately 5% each). Aggregating across all six chokepoints, the total dividend under a 100% risk premium implies trade-cost savings equivalent to thousands of km-equivalent per port pair, translating to tens of billions of dollars annually at current trade volumes.

This finding formalizes the intuition from the international relations and defense eco-

nomics literatures ([Bueger et al., 2019; Kraska, 2015](#)): the U.S. Navy’s forward presence at major chokepoints generates substantial positive externalities for the global trading system. Crucially, the marginal value of security provision is *increasing in the risk environment*: the dividend is largest precisely when security conditions are deteriorating. This has implications for burden-sharing debates: as risk levels rise (due to piracy, conflict spillovers, or geopolitical tensions), the economic case for sustained security investment strengthens rather than weakens ([One Earth Future Foundation, 2010; Mbekeani and Ncube, 2011](#)).

Heterogeneity across ports. The port vulnerability analysis (Section 4.5) reveals that the dividend is not uniformly distributed. Bypass-dependent ports (Black Sea) benefit most from their chokepoint’s security, as they face the largest per-route rerouting costs when forced onto the expensive Constanta–Piraeus overland bypass at $5\times$ normal cost. Corridor-dependent ports (Mediterranean, South Asian, East African) benefit from the security of multiple chokepoints along their primary trade routes. Highly connected hub ports (Rotterdam, New York, Singapore) are relatively insulated, benefiting primarily from the general reduction in risk premiums. This heterogeneity implies that the political economy of maritime security investment is complex: the ports that benefit most from the public good are often in developing regions with limited capacity to contribute to its provision ([Gaubert et al., 2025; Fajgelbaum et al., 2019](#)).

5.2 Structural Patterns and Downstream Implications

Network topology and vulnerability. The expanded 78-node network reveals a structural distinction between two types of chokepoints that is obscured in simpler models. *Through-corridor chokepoints* (Malacca, Gibraltar, Suez, Bab el-Mandeb, Panama) connect large regions of the network; their closure imposes rerouting costs on many port pairs but does not sever connectivity, because alternative maritime routes (e.g., the Lombok Strait as an alternative to Malacca, or the Cape of Good Hope as an alternative to Suez) absorb rerouted traffic. *Bypass-dependent chokepoints* (Bosporus) are the primary connectors for ports behind them; their closure forces traffic onto expensive overland bypass routes, producing very large per-route cost increases even though the network remains technically connected. This distinction maps onto the theoretical framework of [Fajgelbaum and Schaal \(2020a\)](#), who show that optimal transport networks concentrate investment on high-throughput corridors: through-corridor chokepoints carry the highest traffic precisely because they offer the shortest routes between major economic regions.

The practical implication is that security priorities should differ by chokepoint type. For through-corridor chokepoints, the objective is to minimize rerouting costs by maintaining

capacity and reducing risk premiums. For bypass-dependent chokepoints, the objective is to prevent disruption that forces traffic onto dramatically more expensive alternatives, because even with bypass routes available, the cost multiplier ($5 \times$ normal) produces severe economic impacts for dependent ports. This distinction connects to the congestion externality analysis of Hierons (2024): congestion pricing or capacity investment at through-corridor chokepoints can reduce rerouting costs, whereas bypass-dependent chokepoints require both security provision and continued investment in alternative infrastructure (e.g., overland rail) to mitigate vulnerability.

Nonlinear severity and saturation. The partial degradation analysis reveals that the relationship between disruption severity and cost increase is nonlinear for most chokepoints. For through-corridor chokepoints, the severity curve accelerates at high degradation levels ($\alpha \geq 5$) as rerouting becomes the dominant response. Gibraltar and the Suez Canal exhibit the steepest severity curves, producing mean cost increases exceeding 26% and 12% respectively at $\alpha = 5$, reflecting their role as bottlenecks for Mediterranean trade. For the Strait of Malacca, the severity curve is more moderate because the Lombok Strait absorbs rerouted traffic at relatively lower additional cost. This nonlinearity has implications for security investment: the marginal return to reducing risk is highest at moderate disruption levels, suggesting that maintaining a credible deterrent (even short of complete security) captures most of the available dividend.

Supply chain resilience. Our analysis identifies specific port pairs and corridors that are most vulnerable to disruption, providing a basis for supply-chain risk assessment. The Panama Canal produces the largest mean rerouting cost (17,840 km-equivalent) when closed, reflecting the enormous detour required for Atlantic–Pacific traffic. The Suez Canal, as the primary corridor for Asia–Europe trade, produces a mean rerouting cost of 9,949 km when closed, forcing traffic via the Cape of Good Hope or through the Panama Canal across the Pacific. The Bosphorus produces an analogous pattern for Black Sea ports, which must shift to the Constanta–Piraeus overland rail bypass at five times normal cost, with a mean rerouting cost of 3,275 km-equivalent. These findings are consistent with the real-world disruptions documented by Cariou and Cheaitou (2021) during the Ever Given incident and by Verschuur et al. (2023) for broader chokepoint disruption scenarios.

Infrastructure and policy responses. The structural patterns suggest several policy responses, building on the optimal spatial policy framework of Fajgelbaum and Gaubert (2020, 2025). For through-corridor chokepoints, investments that expand capacity or reduce

transit times (canal widening, traffic management systems) can lower baseline costs and reduce the severity of partial disruptions. For bypass-dependent chokepoints, investments in alternative infrastructure—overland rail connections, alternative port development—can reduce the cost multiplier of bypass routes, lowering the vulnerability of dependent ports. The geographic sorting dynamics studied by [Desmet and Henderson \(2015\)](#) and the agglomeration mechanisms of [Duranton and Puga \(2004\)](#) suggest that such investments may also affect the long-run spatial distribution of economic activity, as firms and workers adjust their location decisions in response to changed trade-cost structures.

5.3 Limitations

We are explicit about several limitations that constrain the interpretation of our results, while noting that each suggests a concrete direction for future work.

Static aggregate density. The AIS data aggregate vessel positions from January 2015 to February 2021 into a single snapshot. We cannot track changes in shipping patterns over time, seasonal variations, or the dynamic adjustment to disruptions. A dataset with temporal disaggregation would enable analysis of how trade routes evolve in response to shocks ([Cariou and Cheaitou, 2021](#); [Du et al., 2020](#)).

Aggregate density versus vessel-level flows. The density raster records total AIS positions without distinguishing vessel type, flag, cargo, or voyage. We cannot weight traffic by economic value or estimate bilateral trade flows. Extending the analysis to vessel-level AIS data would enable construction of origin-destination trade matrices and support estimation of the full spatial equilibrium model ([Fajgelbaum and Schaal, 2020a](#); [Allen and Arkolakis, 2022](#); [Kerbl, 2022](#)).

No welfare computation. Without bilateral trade volumes and demand elasticities, we cannot compute welfare changes in the general-equilibrium sense of [Redding and Rossi-Hansberg \(2017\)](#) or [Allen and Arkolakis \(2025\)](#). Our delta-cost measures are informative about the direction and relative magnitude of disruption impacts but are not welfare estimates. Connecting our scenario engine to a gravity-based trade model would close this gap.

Exogenous security parameters. The security risk analysis treats risk premiums as exogenous inputs. In reality, security provision is endogenous to the strategic environment: naval deployment decisions respond to threat assessments, which in turn depend on shipping

patterns and insurance pricing (Besley et al., 2015; Kraska, 2015). Endogenizing security provision would require a game-theoretic extension in which a security provider allocates resources across chokepoints to minimize expected trade-cost losses (Rossi-Hansberg, 2004; Fajgelbaum and Gaubert, 2020).

5.4 Directions for Future Research

1. **Vessel-level AIS trajectories.** Access to individual vessel tracks would enable construction of origin-destination trade flow matrices and support estimation of route-choice models with probabilistic assignment (Fajgelbaum and Schaal, 2020a,b).
2. **Bilateral maritime trade data.** Combining vessel-level AIS with customs or port-authority trade data would enable calibration of a full spatial equilibrium model with endogenous demand (Redding and Rossi-Hansberg, 2017; Allen and Arkolakis, 2025; Redding, 2025).
3. **Insurance and risk pricing data.** War-risk insurance premiums and piracy incidence records would provide empirically grounded values for the security parameters (Besley et al., 2015; One Earth Future Foundation, 2010).
4. **Naval presence proxies.** Open-source data on naval deployments and patrol schedules would enable causal estimation of the security provision effect (Proost and Thisse, 2019).
5. **Dynamic extensions.** A time-varying network with stochastic disruptions and adjustment costs would capture the temporal dimension of chokepoint risk, including the option value of maintaining alternative routes (Hierons, 2024; Bordeu, 2025). Such a model could incorporate the geographic sorting dynamics of Desmet and Henderson (2015) and the agglomeration mechanisms of Duranton and Puga (2004).
6. **Optimal security allocation.** A normative extension could solve for the optimal spatial allocation of security resources, building on Fajgelbaum and Gaubert (2020, 2025) and Gaubert et al. (2025). This would address: given a fixed security budget, which chokepoints should receive the most protection?
7. **Political economy of burden-sharing.** The observation that maritime security is a global public good with concentrated provision raises questions about sustainability and equity. An extension incorporating political-economy considerations (Fajgelbaum et al., 2019; Bordeu, 2025) could analyze the efficiency and distributional consequences of alternative burden-sharing regimes.

5.5 Conclusion

Maritime security is a global public good whose economic value has been under-studied relative to its importance. This paper contributes a transparent, replicable framework for measuring chokepoint vulnerability and quantifying the hegemonic dividend from security provision. Using AIS density data from the IMF, we constructed a 78-node maritime transport network with 1,540 port-to-port trade routes and implemented a multi-scenario stress-testing engine.

Three main findings emerge. First, chokepoint disruptions produce large and heterogeneous trade-cost increases: the Panama Canal (mean rerouting cost of 17,840 km-equivalent), Gibraltar (10,624 km), and the Suez Canal (9,949 km) generate the largest rerouting costs when fully closed, while the bypass-dependent Bosphorus forces Black Sea ports onto an expensive overland alternative at $5\times$ normal maritime cost. Second, the marginal value of security provision is increasing in the risk environment: the hegemonic dividend is largest precisely when security conditions are deteriorating. Third, the vulnerability is highly heterogeneous across ports, with bypass-dependent ports and corridor-dependent developing-region ports benefiting most from the global public good of maritime security. Our cost-per-day estimates—ranging from \$16 million to \$233 million per day depending on the chokepoint—provide a concrete, policy-relevant metric for evaluating the economic value of maritime security provision.

These findings are offered as a data-grounded first step that identifies the data requirements and modeling extensions needed for a full causal assessment of the economic value of maritime security. The orders of magnitude—rerouting costs translating to tens of billions of dollars annually, with the most affected port pairs facing cost increases of 10,000–18,000 km-equivalent—suggest that the economic stakes of maritime security provision are substantial, and that the hegemonic dividend from concentrated security at critical chokepoints is a first-order feature of the global trading system (Bueger et al., 2024; Rossi-Hansberg et al., 2023; Owens et al., 2020).

References

- Allen, T. and Arkolakis, C. (2022). The welfare effects of transportation infrastructure improvements. *Review of Economic Studies*, 89(6):2911–2957.
- Allen, T. and Arkolakis, C. (2025). Quantitative regional economics. In *Handbook of Urban and Regional Economics*, volume 6, chapter 1. Elsevier.

- Besley, T., Fetzer, T., and Mueller, H. (2015). The welfare cost of lawlessness: Evidence from Somali piracy. *Journal of the European Economic Association*, 13(6):979–997.
- Bordeu, O. (2025). Commuting infrastructure in fragmented cities. Working Paper.
- Bueger, C., Edmunds, T., and Ryan, B. J. (2019). Maritime security: The uncharted politics of the global sea. *International Affairs*, 95(5):971–978.
- Bueger, C., Edmunds, T. P., and Stockbruegger, J. (2024). Securing the seas: A comprehensive assessment of global maritime security. Technical report, SafeSeas.
- Cariou, P. and Cheaitou, A. (2021). The use of AIS data to analyse the economic impact of disruptive events on container flows and ship waiting times in main ports. *Maritime Economics & Logistics*, 23(4):605–625.
- Cerdeiro, D. A. and Komaromi, A. (2020). Nowcasting world trade using AIS data: A machine learning approach. *IMF Working Paper*, (WP/20/90).
- Cerdeiro, D. A., Komaromi, A., Liu, Y., and Saeed, M. (2020). World seaborne trade in real time: A proof of concept for building AIS-based nowcasts from scratch. IMF Working Paper WP/20/57, International Monetary Fund.
- Desmet, K. and Henderson, J. V. (2015). The geography of development within countries. In *Handbook of Regional and Urban Economics*, volume 5, chapter 22. Elsevier.
- Donaldson, D. (2025). Transport infrastructure and policy evaluation. In *Handbook of Regional and Urban Economics*, volume 6, chapter 5, pages 287–352. Elsevier.
- Du, Y., Wang, S., and Meng, Q. (2020). How are ports tackling congestion and delays? *Maritime Policy & Management*, 47(5):603–617.
- Duranton, G. and Puga, D. (2004). Micro-foundations of urban agglomeration economies. In *Handbook of Regional and Urban Economics*, volume 4, chapter 48. Elsevier.
- Fajgelbaum, P. D. and Gaubert, C. (2020). Optimal spatial policies, geography, and sorting. *Quarterly Journal of Economics*, 135(2):959–1036.
- Fajgelbaum, P. D. and Gaubert, C. (2025). Optimal spatial policies. In *Handbook of Urban and Regional Economics*, volume 6, chapter 3. Elsevier.
- Fajgelbaum, P. D., Morales, E., Suárez Serrato, J. C., and Zidar, O. (2019). State taxes and spatial misallocation. *Review of Economic Studies*, 86(1):333–376.

- Fajgelbaum, P. D. and Schaal, E. (2020a). Optimal transport networks in spatial equilibrium. *Econometrica*, 88(4):1411–1452.
- Fajgelbaum, P. D. and Schaal, E. (2020b). Supplement to “Optimal Transport Networks in Spatial Equilibrium”. *Econometrica Supplementary Material*, 88(4).
- Gaubert, C., Kline, P., and Yagan, D. (2025). Place-based redistribution. Working Paper.
- Hierons, T. (2024). Spreading the jam: Optimal congestion pricing in general equilibrium. Working Paper.
- Kerbl, S. (2022). Economic research with AIS data. *CESifo Forum*, 23(1):43–47.
- Kraska, J. (2015). Law of the sea. In *The Oxford Handbook of the Use of Force in International Law*. Oxford University Press.
- Mbekeani, K. K. and Ncube, M. (2011). Economic impact of maritime piracy. Africa Economic Brief 10, African Development Bank.
- Morabito, G. (2023). *Maritime Transport Economics and Policy*. PhD thesis, University of Messina.
- Notteboom, T. E. (2006). The impact of port congestion on freight rates and the shipping industry. *Journal of Transport Geography*, 14(3):197–212.
- One Earth Future Foundation (2010). The economic cost of piracy. Technical report, Oceans Beyond Piracy.
- Owens, R., Rossi-Hansberg, E., and Sarte, P.-D. (2020). Rethinking Detroit. *American Economic Journal: Economic Policy*, 12(2):258–305.
- Proost, S. and Thisse, J.-F. (2019). What can be learned from spatial economics? *Journal of Economic Literature*, 57(3):575–643.
- Redding, S. J. (2025). Quantitative urban economics. In *Handbook of Urban and Regional Economics*, volume 6, chapter 2. Elsevier.
- Redding, S. J. and Rossi-Hansberg, E. (2017). Quantitative spatial economics. *Annual Review of Economics*, 9:21–58.
- Rossi-Hansberg, E. (2004). Optimal urban land use and zoning. *Review of Economic Dynamics*, 7(1):69–106.

- Rossi-Hansberg, E. (2020). Transportation networks. Lecture slides, University of Chicago.
- Rossi-Hansberg, E., Sarte, P.-D., and Schwartzman, F. (2023). Cognitive hubs and spatial redistribution. *American Economic Journal: Macroeconomics*, 15(3):254–299.
- Verschuur, J., Lumma, J., and Hall, J. W. (2023). Systemic impacts of disruptions at maritime chokepoints. *Nature Communications*, 14(1):5945.

A Chokepoint Bounding Box Maps

Figure 18 shows all six chokepoint bounding boxes on a single world map. Figures 19–24 show individual zoomed maps for each chokepoint, with the AIS density visible in the background and the bounding box coordinates annotated.

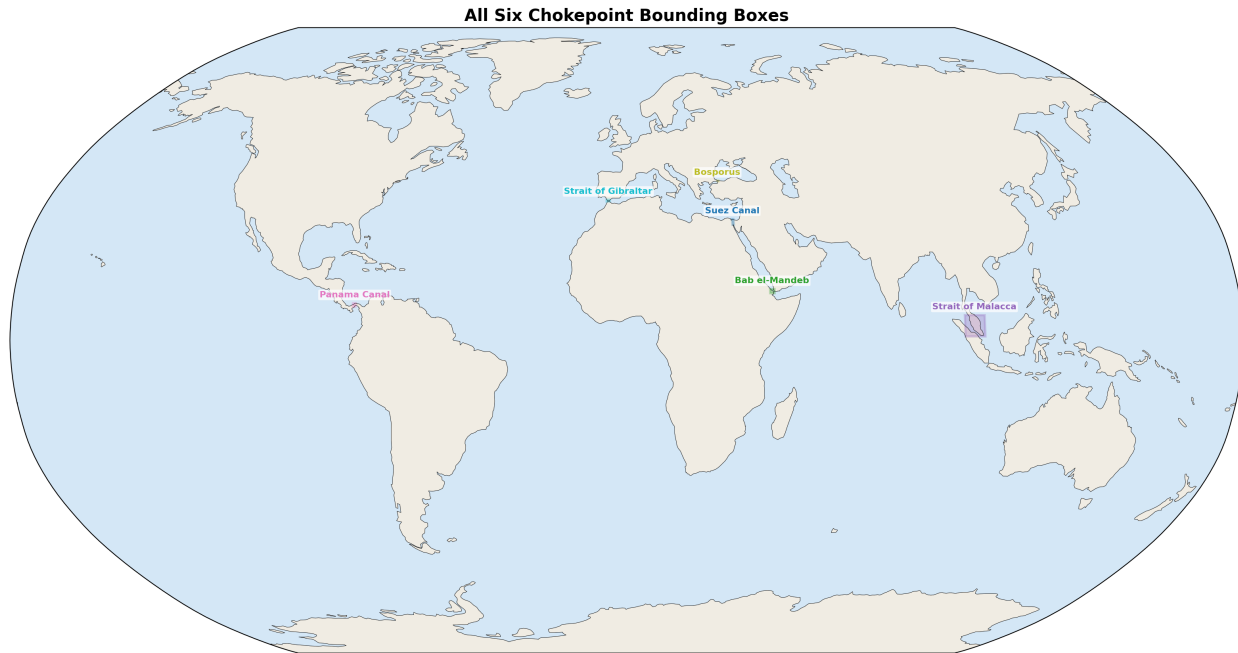


Figure 18: All six chokepoint bounding boxes overlaid on a world map.

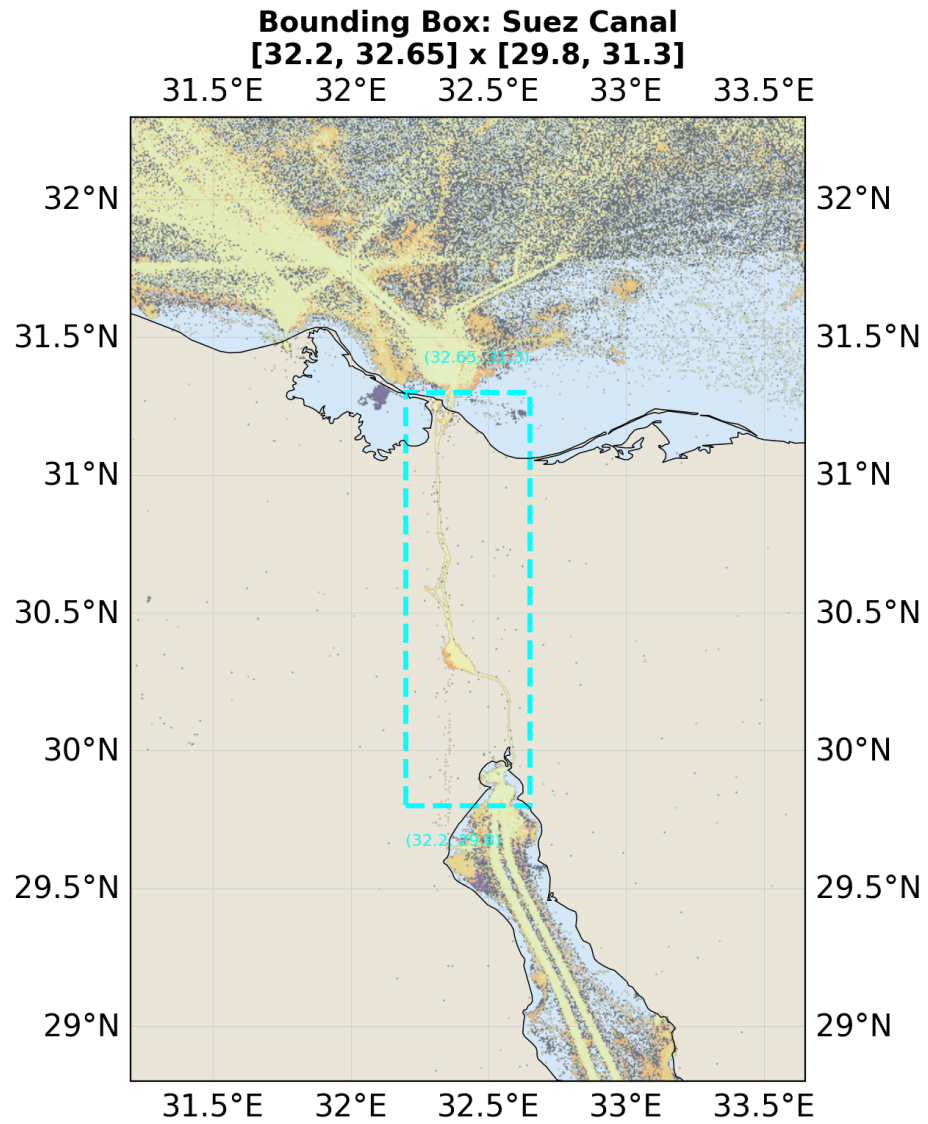


Figure 19: Bounding box: Suez Canal.

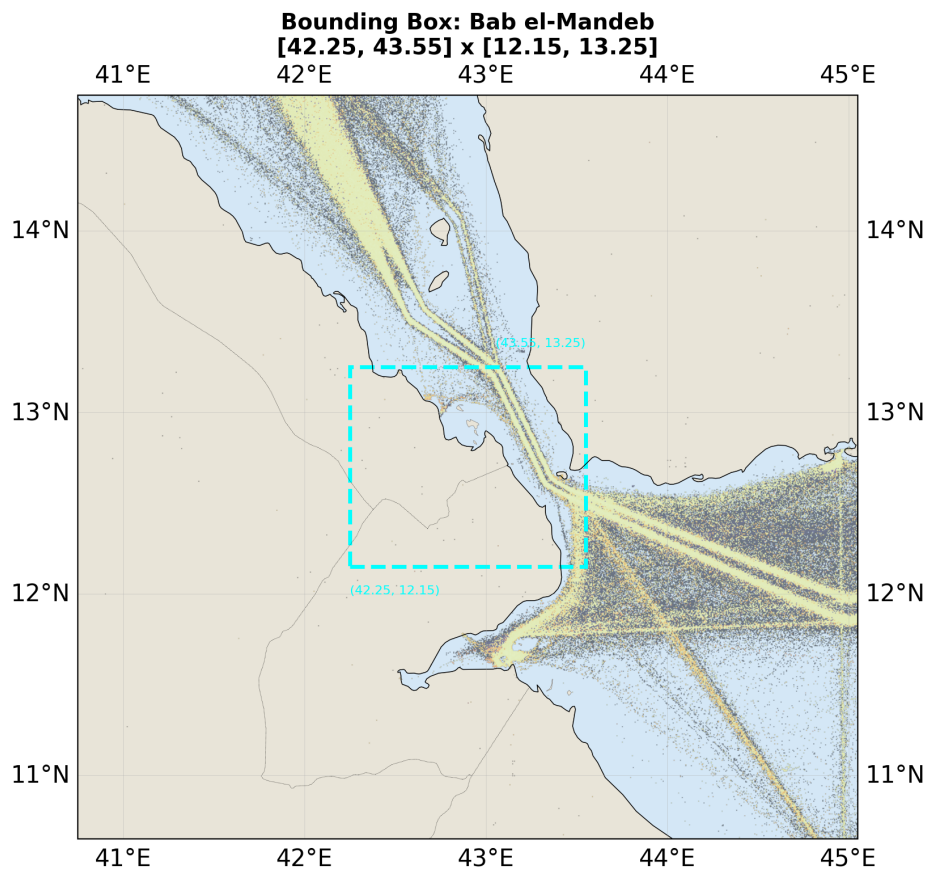


Figure 20: Bounding box: Bab el-Mandeb.

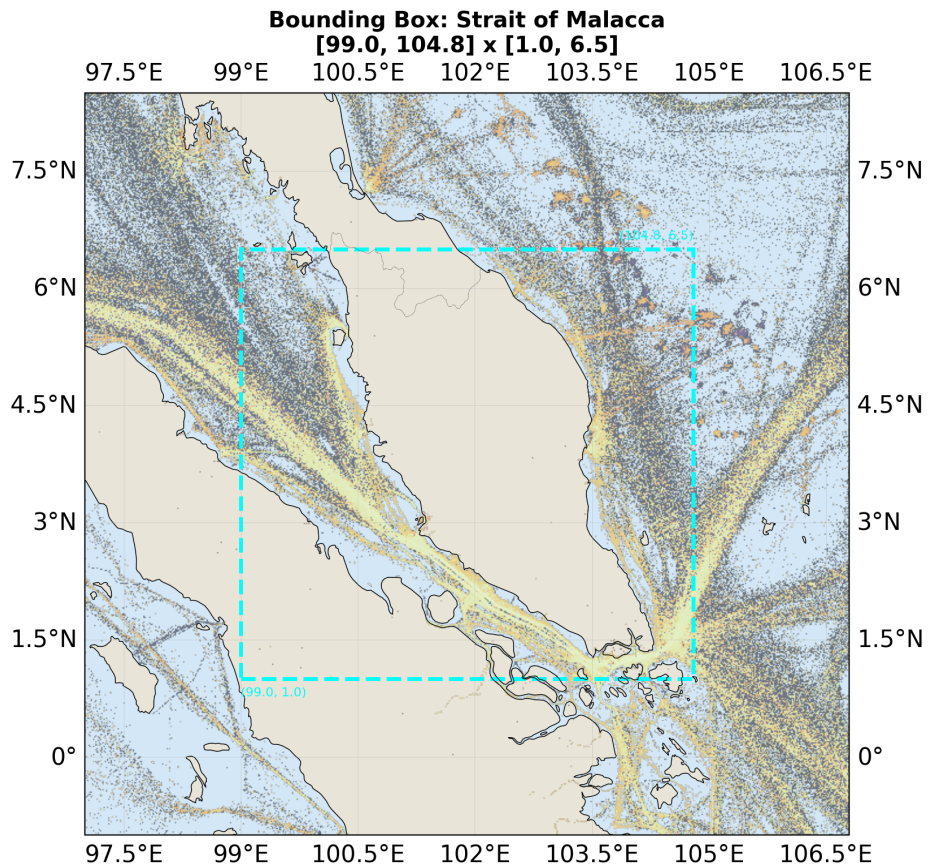


Figure 21: Bounding box: Strait of Malacca.

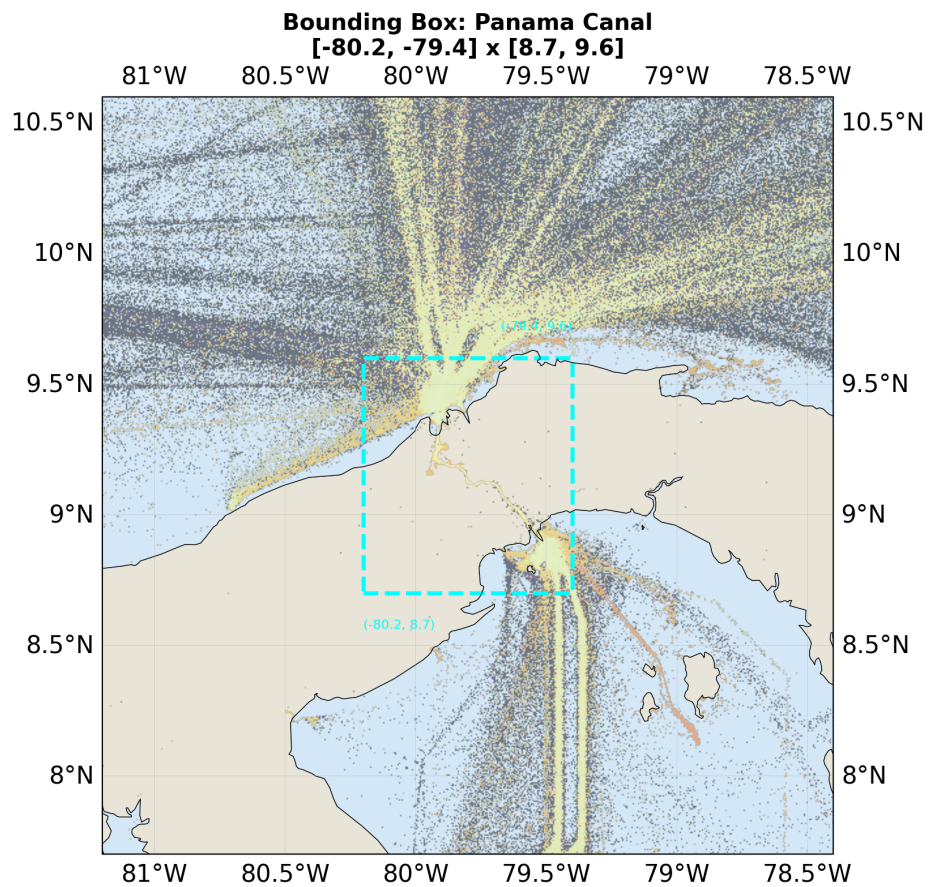


Figure 22: Bounding box: Panama Canal.

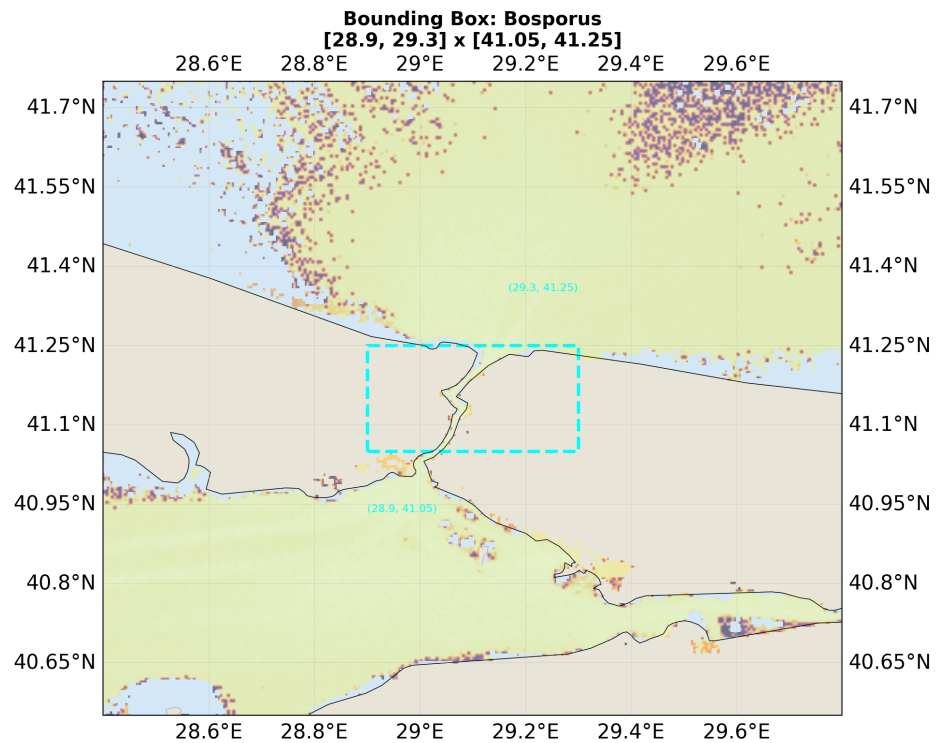


Figure 23: Bounding box: Bosphorus.

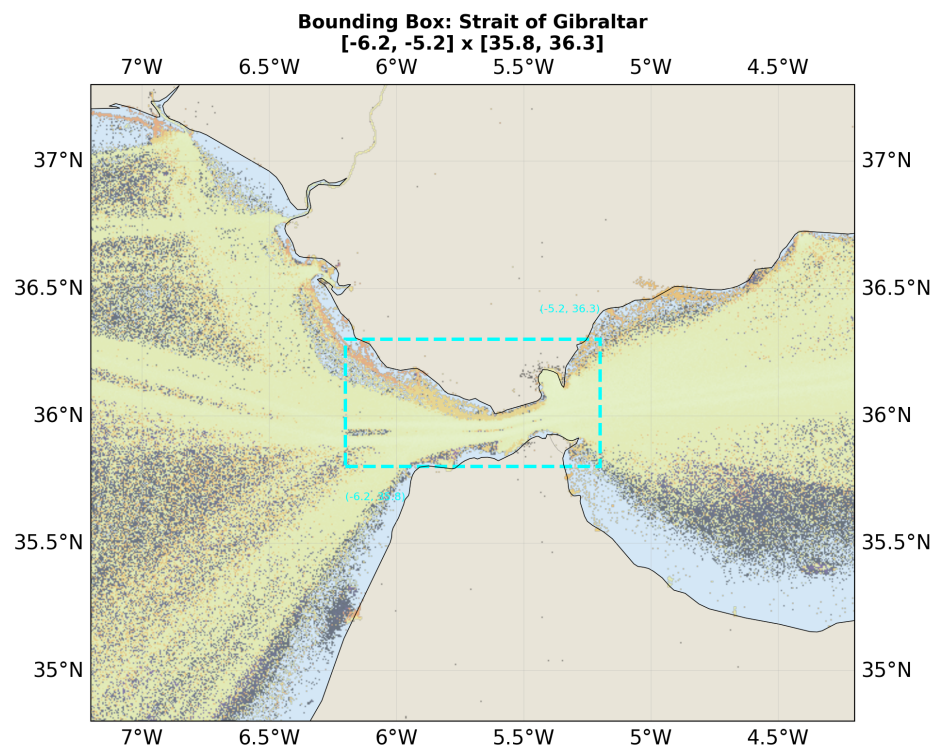


Figure 24: Bounding box: Strait of Gibraltar.

B Chokepoint Traffic Density Close-ups

Figures 25–30 show zoomed AIS density overlays for each chokepoint bounding box, with intensity statistics annotated.

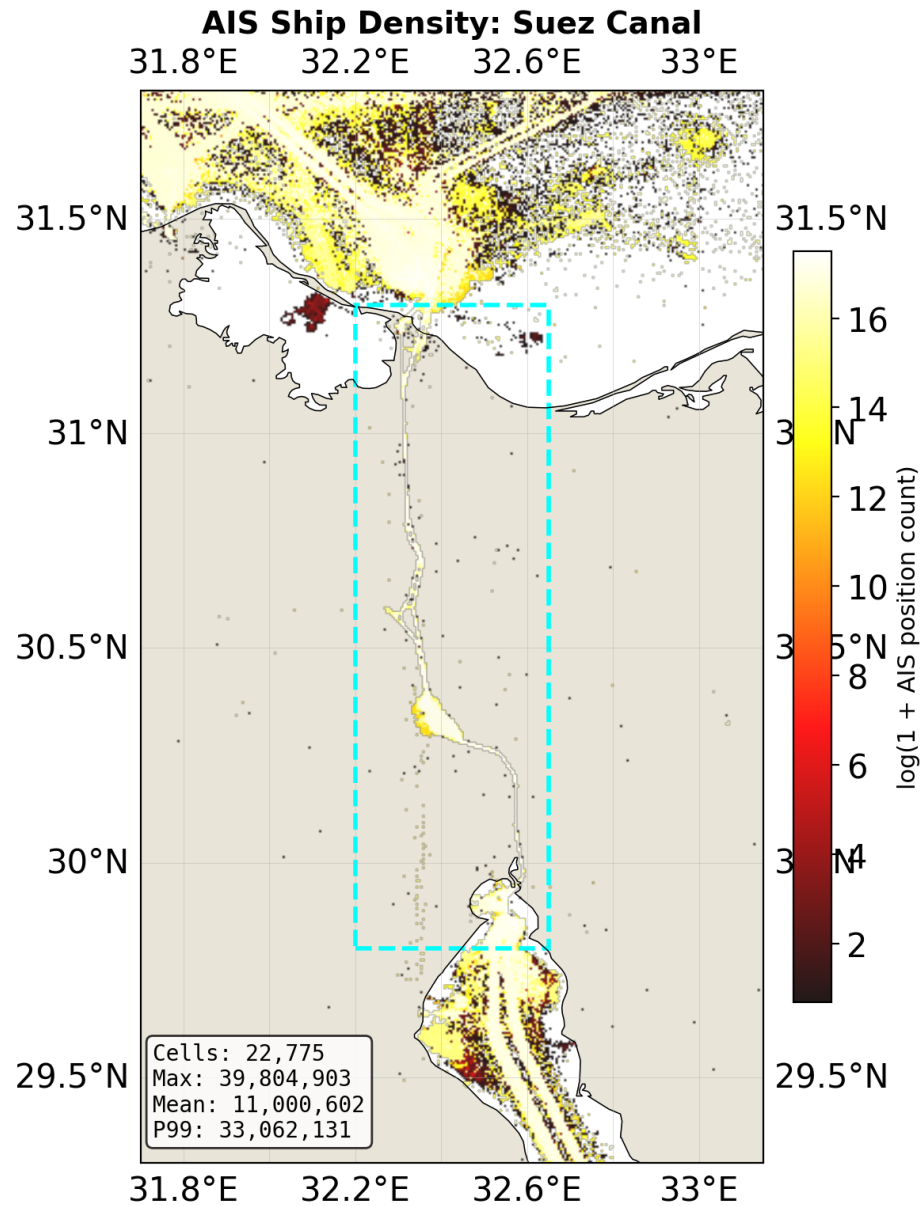


Figure 25: AIS density: Suez Canal.

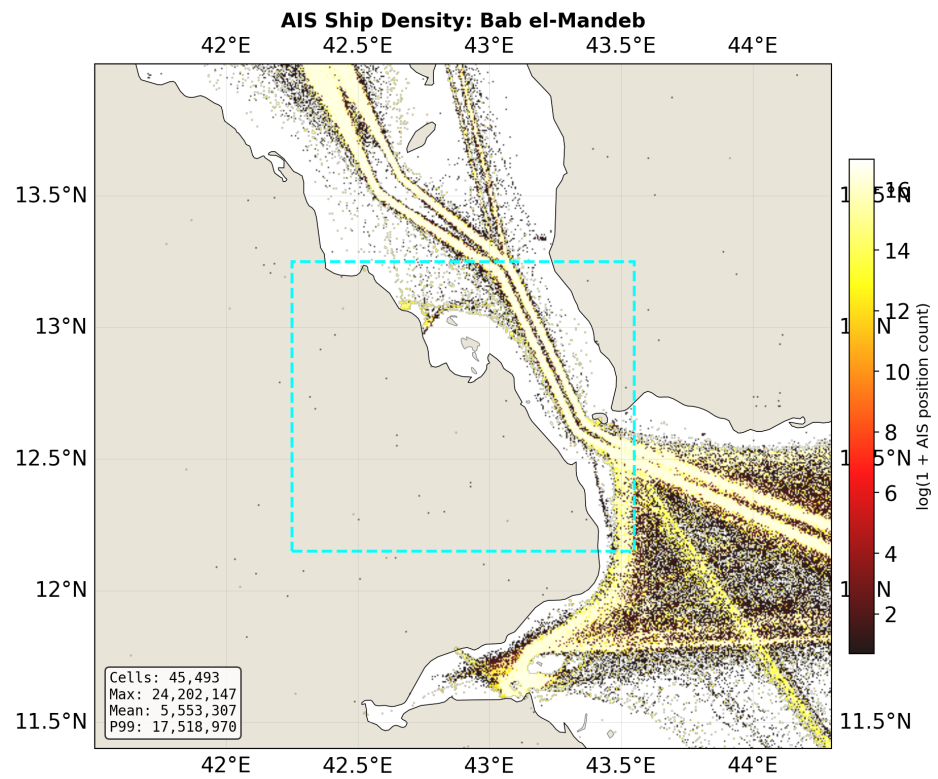


Figure 26: AIS density: Bab el-Mandeb.

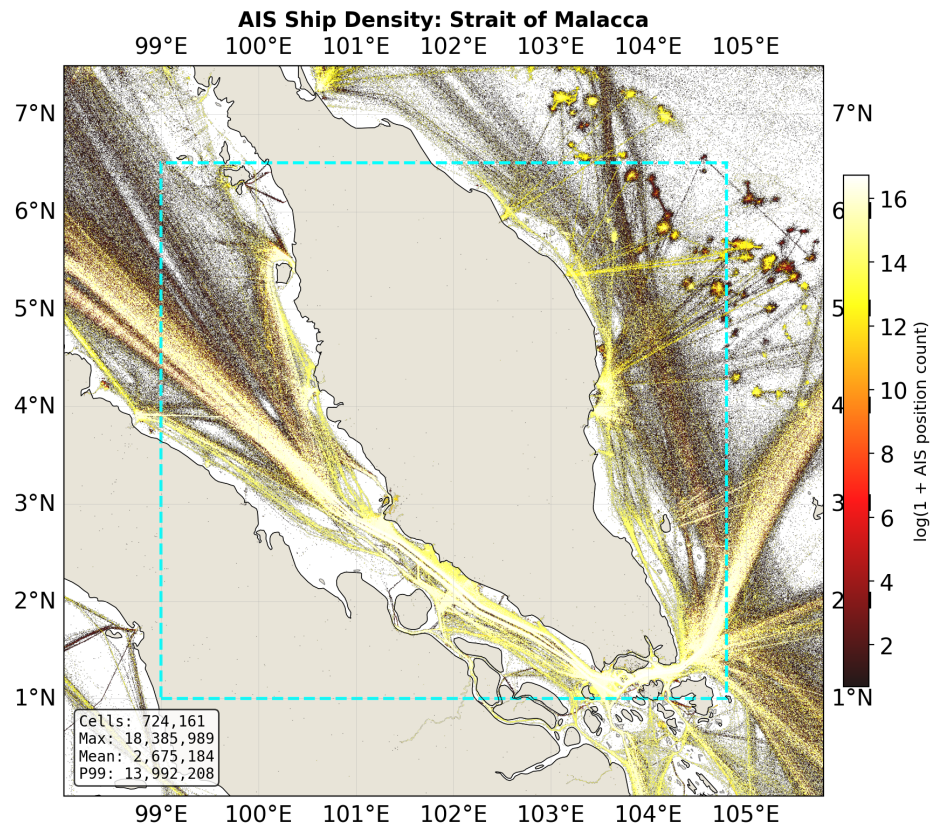


Figure 27: AIS density: Strait of Malacca.

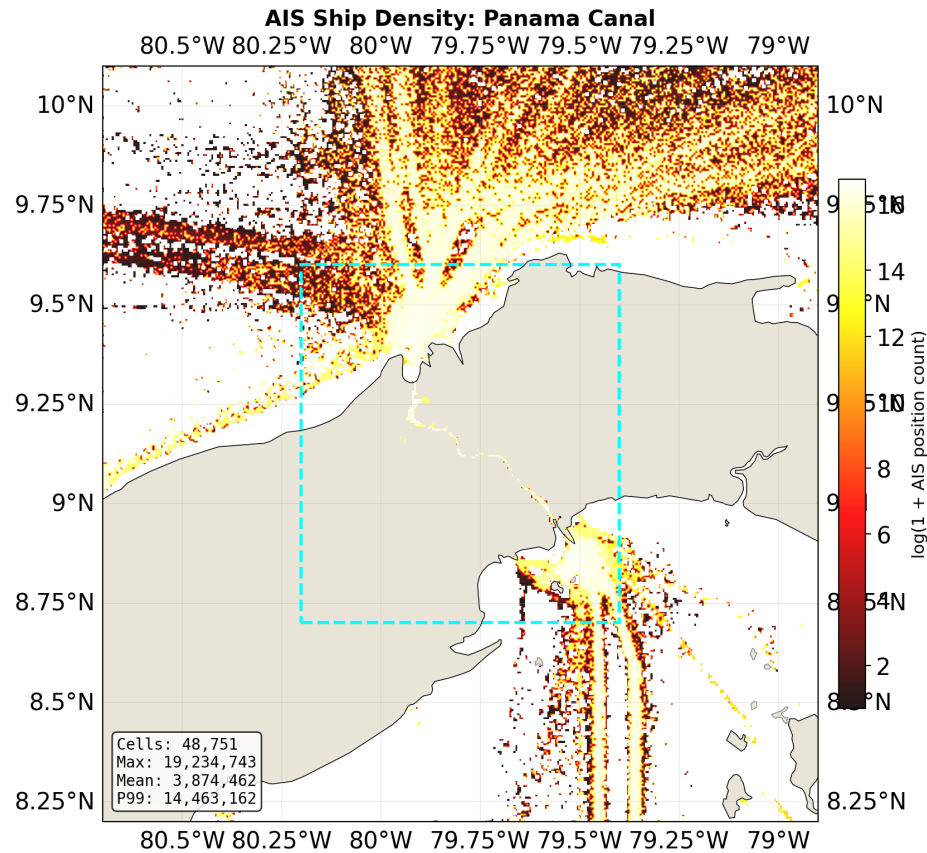


Figure 28: AIS density: Panama Canal.

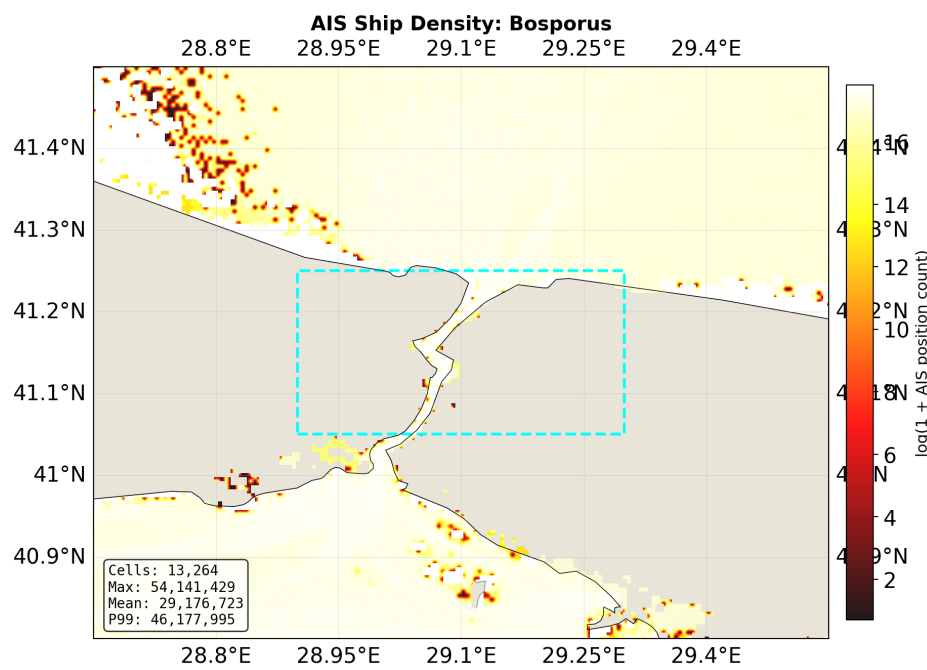


Figure 29: AIS density: Bosphorus.

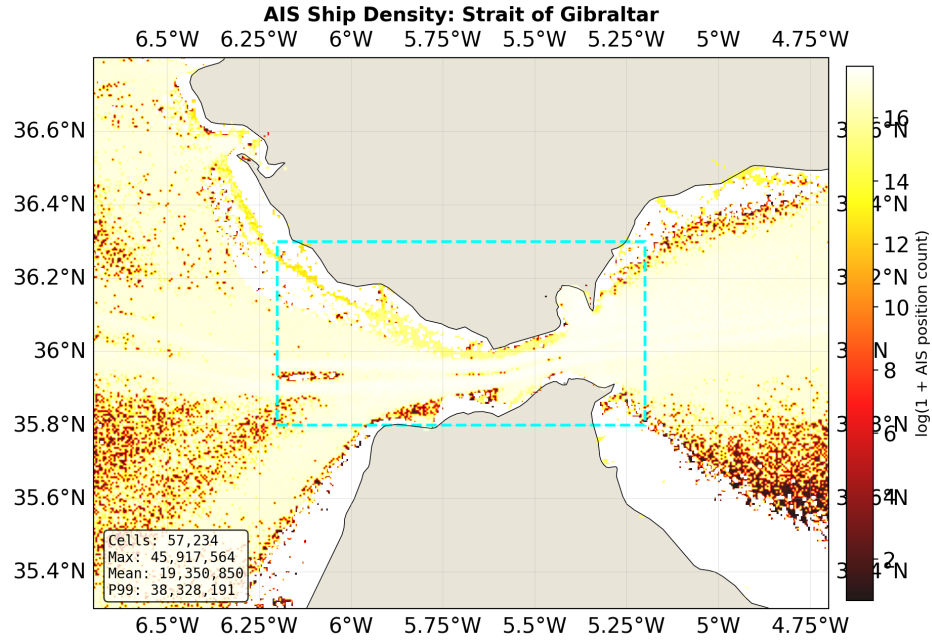


Figure 30: AIS density: Strait of Gibraltar.

C Chokepoint Descriptive Statistics

The full chokepoint intensity table is reported below, followed by four-panel descriptive statistics figures for each chokepoint.

Table 5: Chokepoint traffic intensity from AIS raster data. Sum intensity reflects total vessel traffic density within each chokepoint bounding box.

Chokepoint	Sum Intensity	Mean Intensity	P99 Cell	Grid Cells	Rank
Strait of Malacca	1.21T	945.8K	12.61M	1,276,000	1
Gibraltar	249.01B	12.45M	40.31M	20,000	2
Bab el Mandeb	46.04B	804.9K	15.90M	57,200	3
Panama Canal	40.36B	1.40M	15.39M	28,800	4
Suez Canal	35.79B	1.33M	32.09M	27,000	5
Bosporus	11.36B	3.55M	48.42M	3,200	6

Chokepoint Analysis: Suez Canal

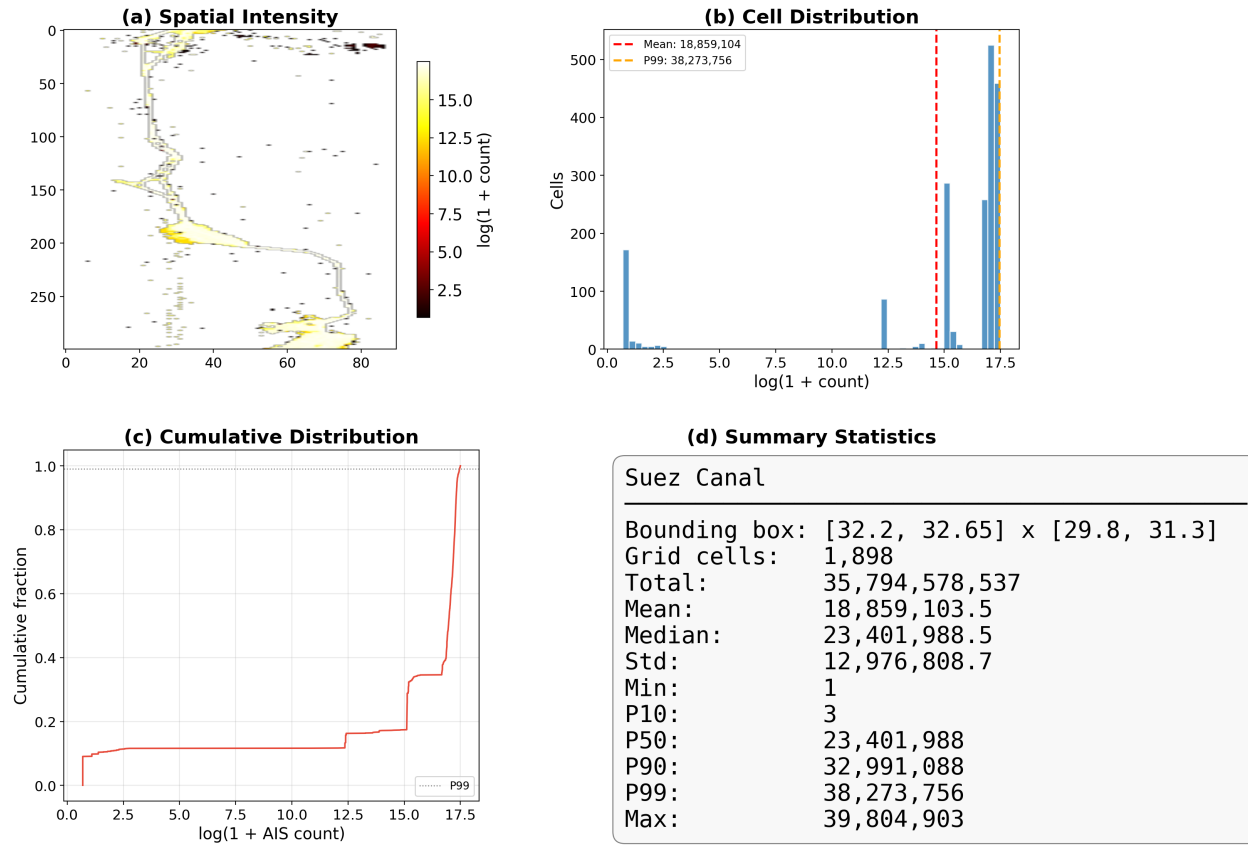


Figure 31: Descriptive statistics: Suez Canal.

Chokepoint Analysis: Bab el-Mandeb

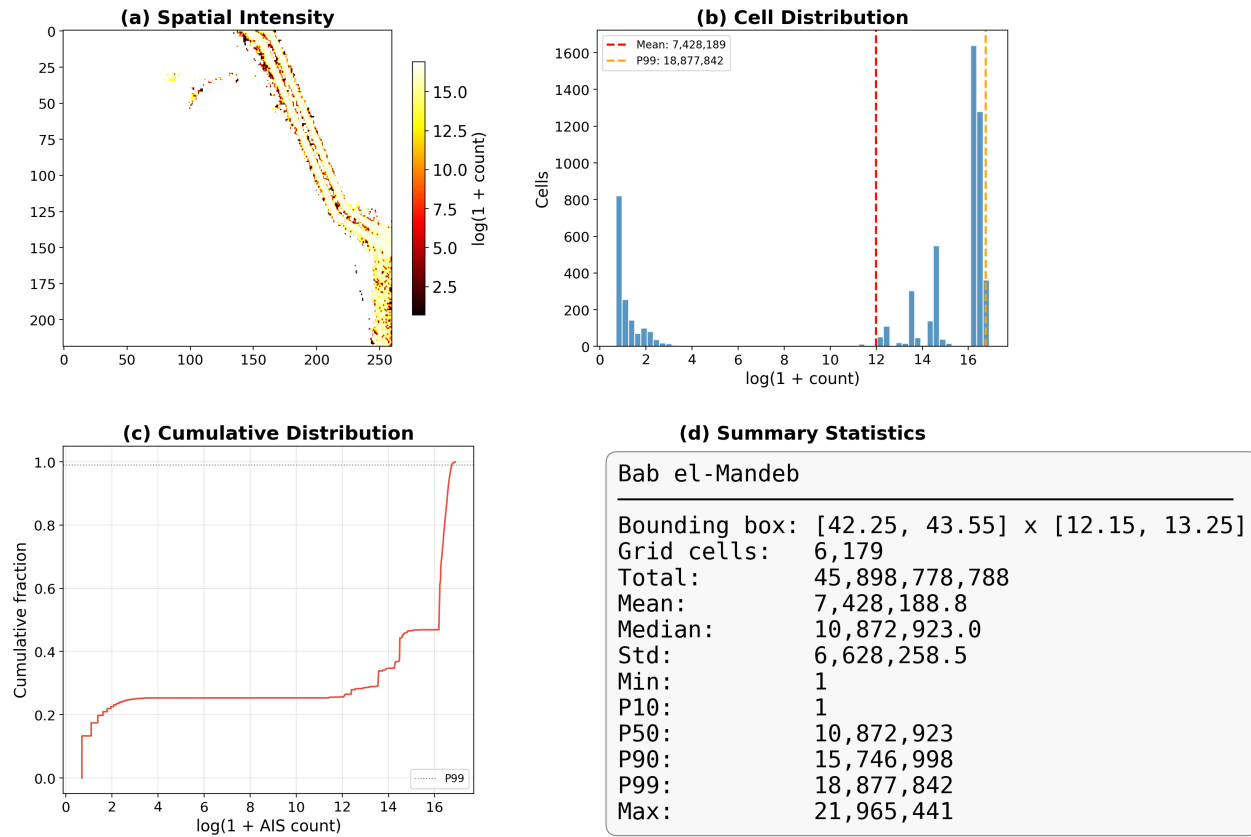


Figure 32: Descriptive statistics: Bab el-Mandeb.

Chokepoint Analysis: Strait of Malacca

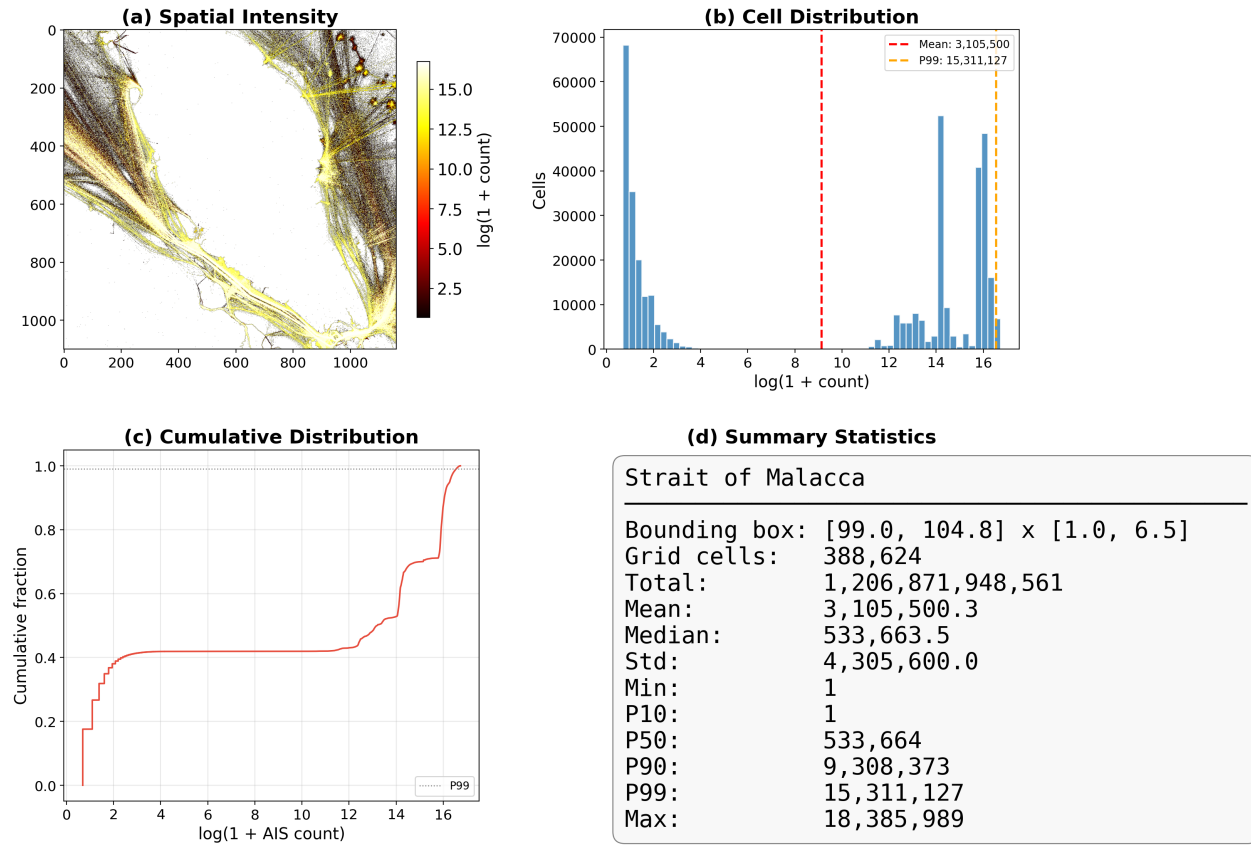


Figure 33: Descriptive statistics: Strait of Malacca.

Chokepoint Analysis: Panama Canal

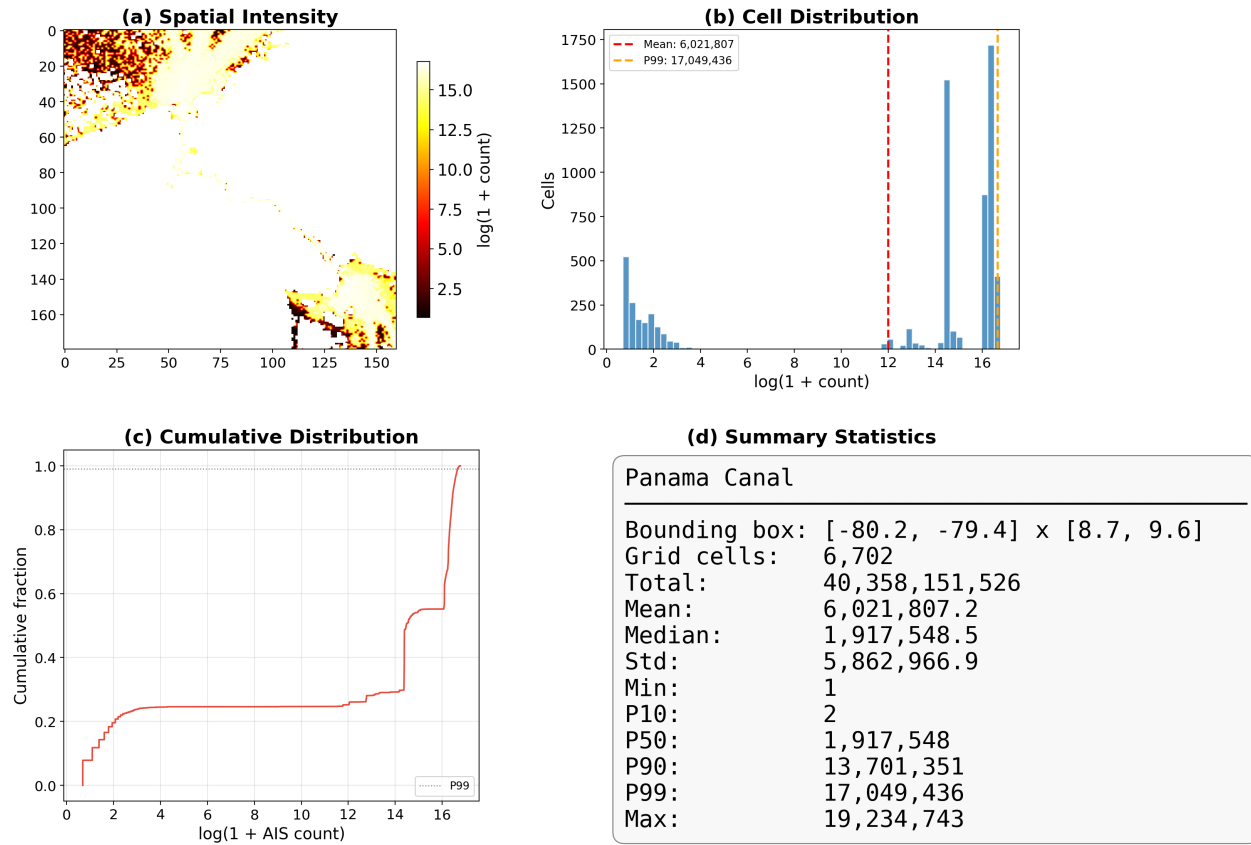


Figure 34: Descriptive statistics: Panama Canal.

Chokepoint Analysis: Bosphorus

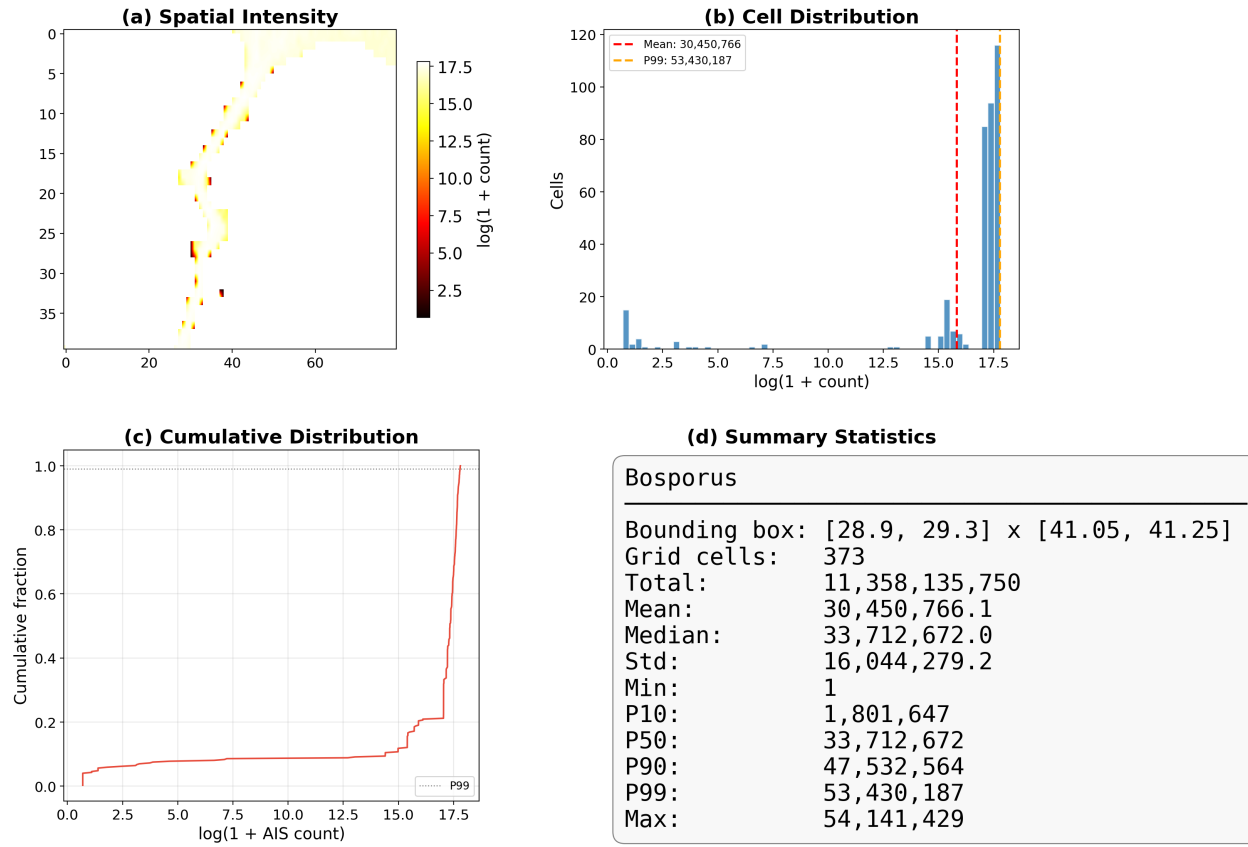


Figure 35: Descriptive statistics: Bosphorus.

Chokepoint Analysis: Strait of Gibraltar

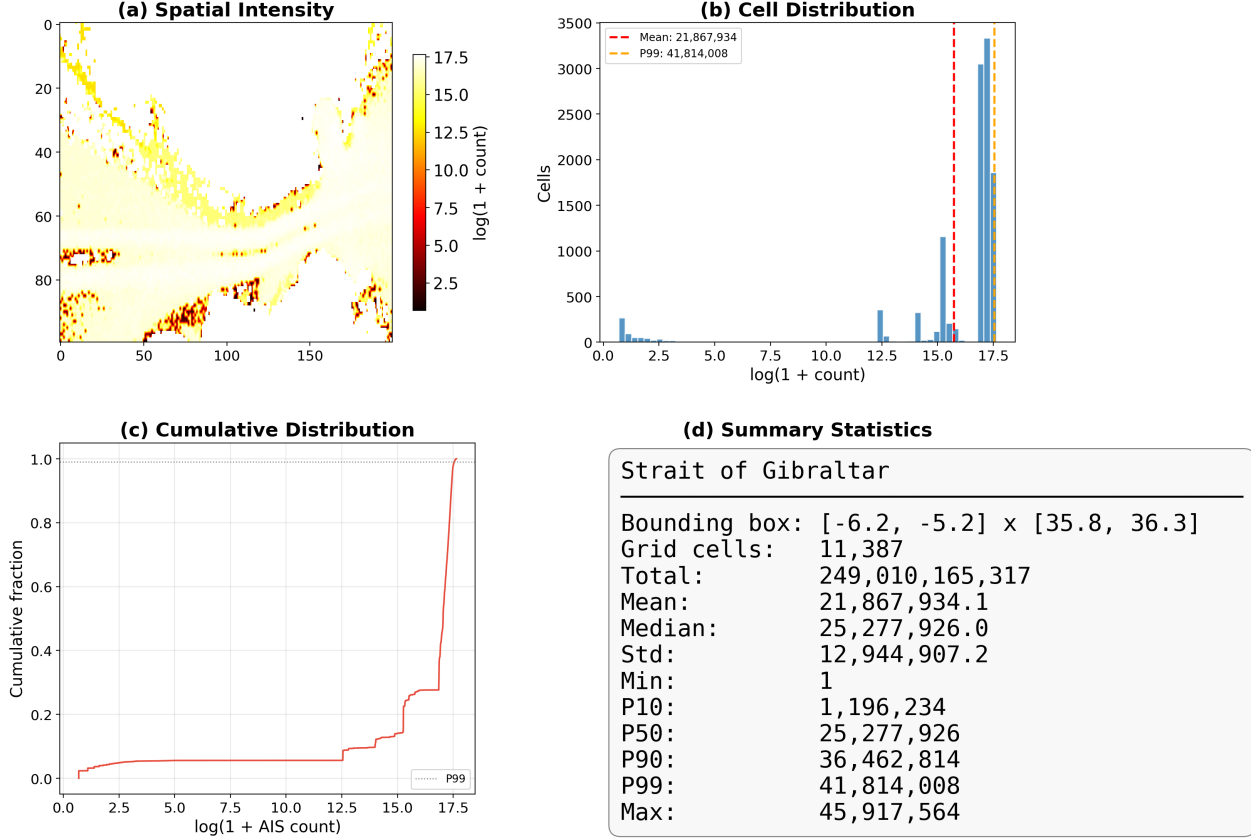


Figure 36: Descriptive statistics: Strait of Gibraltar.

D Ship-Count Estimation Under Closure Scenarios

D.1 Baseline Annual Transit Estimates

To translate our network-based rerouting costs into concrete operational magnitudes, we estimate the number of vessels affected by each chokepoint closure scenario. We draw baseline annual transit counts from published sources—canal authority statistics, UNCTAD reports, and U.S. Energy Information Administration (EIA) data—rather than attempting to reverse-engineer vessel counts from our aggregate AIS density raster, which records cumulative position reports without distinguishing individual vessel transits.

Table 6 reports the baseline annual transit estimates for each chokepoint, along with the data source and the approximate range reflecting inter-year variation over the 2015–2021 period.

Table 6: Estimated annual vessel transits at each chokepoint. Ranges reflect inter-year variation over 2015–2021 and rounding uncertainty.

Chokepoint	Central Estimate	Range	Source
Strait of Gibraltar	80,000	70,000–100,000	UNCTAD, Verschuur et al. (2023)
Strait of Malacca	85,000	80,000–94,000	IMO, UNCTAD
Bosporus	43,000	40,000–46,000	Turkish Directorate General
Bab el-Mandeb	25,000	20,000–30,000	UNCTAD, EIA
Suez Canal	19,500	18,000–20,700	Suez Canal Authority
Panama Canal	13,500	12,000–14,500	Panama Canal Authority

Several caveats apply to these estimates. First, “transits” count individual vessel passages through the chokepoint; a vessel that makes multiple round trips during a year is counted multiple times. Second, transit counts include all vessel types (container ships, tankers, bulk carriers, military vessels, fishing vessels, passenger ships), not only cargo-carrying vessels relevant to trade. Third, the AIS density data in our primary analysis include vessel *positions* (typically broadcast every 2–10 seconds), which are far more numerous than vessel transits. The distinction between cumulative AIS position counts and discrete vessel transits is critical: a single vessel transiting a chokepoint bounding box generates thousands to tens of thousands of AIS position reports depending on the transit duration and broadcast frequency.

D.2 Vessels Affected by Closure Scenarios

We estimate the number of vessels affected by each closure scenario by combining the baseline transit counts with the fraction of port pairs affected from our full closure analysis (Section 4.3). For each chokepoint b , the fraction of port pairs affected is $f_b = \text{Pairs Affected}_b / 1,540$. We multiply this fraction by the annual transit count to produce an *order-of-magnitude* estimate of vessels requiring rerouting.

This approach rests on two simplifying assumptions that we state explicitly:

1. **Uniform traffic distribution:** We assume that vessel transits are approximately uniformly distributed across port pairs that use the chokepoint. In reality, a small number of high-volume trade corridors (e.g., Asia–Europe via Suez) dominate transit counts, so the actual number of affected vessels could be higher or lower than our estimate depending on whether high-volume pairs are disproportionately affected.
2. **Transit–pair proportionality:** We assume that the fraction of transits affected is proportional to the fraction of port pairs affected. This would be exact if all port pairs

generated equal traffic volumes, which is clearly not the case. We therefore report our estimates as order-of-magnitude bounds.

Table 7 reports the estimated vessels affected under each full closure scenario.

Table 7: Estimated annual vessels affected by chokepoint closure. Lower and upper bounds reflect the uncertainty range in baseline transit counts. “Rerouted” vessels must find alternative maritime routes; no vessels are fully disconnected under our network design (bypass routes exist for all chokepoints).

Chokepoint Closed	Pairs Affected (%)	Central Est.	Lower Bound	Upper Bound
Panama Canal	298 (19.4%)	2,600	2,300	2,800
Gibraltar	590 (38.3%)	30,600	26,800	38,300
Suez Canal	469 (30.5%)	5,900	5,500	6,300
Bab el-Mandeb	454 (29.5%)	7,400	5,900	8,800
Bosporus	159 (10.3%)	4,400	4,100	4,700
Strait of Malacca	290 (18.8%)	16,000	15,100	17,700

D.3 Interpretation and Uncertainty

The estimates in Table 7 should be interpreted as rough order-of-magnitude indicators rather than precise predictions. Several sources of uncertainty merit discussion:

- **Traffic concentration:** If the affected port pairs include disproportionately high-volume corridors (e.g., Asia–Europe via Suez), the actual number of affected vessels could be 2–3× higher than our central estimate. Conversely, if the affected pairs are predominantly low-volume routes, the actual number could be lower.
- **Vessel heterogeneity:** Different vessel types respond differently to chokepoint closure. Large container ships and VLCCs (Very Large Crude Carriers) face the highest rerouting costs due to fuel consumption and draft restrictions at alternative routes. Smaller vessels may have more flexibility. Our estimates treat all vessels equally.
- **Dynamic adjustment:** In practice, chokepoint closure would trigger immediate queuing, followed by gradual fleet redeployment to alternative routes. The steady-state number of affected vessels (after adjustment) would differ from the initial impact. Our estimates reflect the steady-state assumption.
- **Temporal variation:** Annual transit counts vary with global trade cycles, seasonal patterns, and geopolitical events. The 2020 COVID-19 pandemic reduced traffic at most chokepoints by 5–15%; conversely, post-pandemic recovery saw record transits at several chokepoints. Our estimates use mid-period averages.

For trade-security assessments, the Suez Canal estimate is particularly policy-relevant. Approximately 19,500 vessels transit the Suez Canal annually, handling roughly 12% of global trade by volume ([Cariou and Cheaitou, 2021](#)). Under our closure scenario, all Suez-dependent traffic must reroute via the Cape of Good Hope or through the Panama Canal, adding a mean of 9,949 km-equivalent to affected routes. The 2021 Ever Given grounding provided a real-world preview of such disruption: even a six-day blockage produced cascading supply-chain effects and measurable increases in shipping costs ([Cariou and Cheaitou, 2021](#); [Verschuur et al., 2023](#)).